Journal of Pharmaceutical Analysis 16 (2026) 101349

Contents lists available at ScienceDirect

Journal of Pharmaceutical Analysis

journal homepage: www.elsevier.com/locate/jpa

Review paper

Recent advances in nanomaterial-based optical biosensors and their biomedical and biopharmaceutical applications

Mengjia Xu [a, b], Lutfun Nahar [c, ***], Kenneth J. Ritchie [d], Chenxu Wang [a], Li Cheng [e], Zimiao Wu [e], Satyajit D. Sarker [d, **], Mingquan Guo [a, *]

[a] Ningbo Key Laboratory of Biomedical Imaging Probe Materials and Technology, Zhejiang International Cooperation Base of Biomedical Materials Technology and Application, Ningbo Cixi Institute of Biomedical Engineering, Laboratory of Advanced Theranostic Materials and Technology, Ningbo Institute of Materials Technology and Engineering, Chinese Academy of Sciences, Ningbo, Zhejiang, 315201, China
[b] College of Food Science and Technology, Nanjing Agricultural University, Nanjing, 210095, China
[c] Laboratory of Growth Regulators, Palacký University and Institute of Experimental Botany, The Czech Academy of Sciences, Olomouc, 78371, Czech Republic
[d] Centre for Natural Products Discovery, School of Pharmacy and Biomolecular Sciences, Liverpool John Moores University, Liverpool, L3 3AF, UK
[e] Affiliated Cixi Hospital, Wenzhou Medical University, Ningbo, Zhejiang, 315300, China

ARTICLE INFO

Article history:
Received 11 November 2024
Received in revised form
11 May 2025
Accepted 15 May 2025
Available online 19 May 2025

Keywords:
Optical biosensors
Low-dimensional nanomaterials
Fundamental mechanisms for biosensing
At-home diagnostics
Continuous molecular monitoring
Biopharmaceutical applications

ABSTRACT

Optical biosensors are gaining popularity owing to their portability, miniaturization, no requirement for additional attachments, and rapid responsiveness. These features render them suitable for various applications including at-home diagnostics, pharmacology, and continuous molecular monitoring. The integration of functionalized low-dimensional nanomaterials (zero-dimensional (0D), 1D, 2D, and 3D) has redirected focus towards the design, fabrication, and optimization of optical biosensors. This review summarizes the fundamental mechanisms underlying optical biosensing. The key mechanisms include localized surface plasmon resonance (LSPR), photoluminescence (PL), surface enhancement Raman scattering (SERS), nanozyme-based colorimetric strategies, chemiluminescence, bioluminescence, and electrochemiluminescence. The advantages of various low-dimensional nanomaterials for different types of optical biosensors are presented. This comparison emphasizes their potential superiority in targeted biosensing applications. Therefore, promoting optical biosensing techniques and recent developments in advanced biosensing strategies for biomedical research and biopharmaceutical applications are necessary to establish their future directions.

1. Introduction

The field of sensing technology is essential for advancing diagnostics and molecular analysis, facilitating innovations with profound impacts on human health. One of the earliest examples of sensing technology is litmus paper for pH detection, which introduced chemical indicators as reliable tools for simple testing methods [1]. Research soon shifted focus to biological molecules, making enzymes central to the development of sensors. In 1962, scientists pioneered a glucose quantification method by combining an electrochemical oxygen sensor with glucose oxidase, paving the way for optical biosensors based on biological recognition molecules [2,3]. For decades, electrochemical sensing methods have remained dominant in the market due to their versatility and commercial adaptability for point-of-care (POC) testing [4]. However, recent advancements, such as miniature optics and automated microfluidics, have transformed optical sensors into practical, commercially viable devices. While electrochemical sensors hold a large market share primarily for glucose monitoring, optical biosensors have emerged as one of the fastest-growing segments, fueled by the expanding demand for lateral flow assays that extend far beyond pregnancy tests [5,6]. In general, an optical biosensor integrates a receptor and transducer to translate biochemical information into measurable signals with high sensitivity and specificity [7]. Compared to electrochemical sensors, optical nanosensors stand out in biomedical and biopharmaceutical monitoring due to their simplicity, portability, and rapid responsiveness [8]. The increase in miniaturized optical equipment, particularly complementary metal-oxide-semiconductor cameras

Peer review under responsibility of Xi'an Jiaotong University.
* Corresponding author.
** Corresponding author.
*** Corresponding author.
E-mail addresses: nahar@ueb.cas.cz (L. Nahar), S.Sarker@ljmu.ac.uk (S.D. Sarker), guomingquan@nimte.ac.cn (M. Guo).

https://doi.org/10.1016/j.jpha.2025.101349

in smartphones, has redefined optical biosensing. Handheld optical readers reduce costs and streamline detection, whereas smartphone cameras serve as signal readouts that link intensity readings to 3D information through digital holography [9]. The rapid advancements in miniature microscopes and real-time diagnostic capabilities are guiding the future of optical sensing.

Over the past decade, breakthroughs in nanomaterials combined with advanced bio-recognition techniques have significantly propelled optical biosensing. Nanomaterials, when conjugated to target ligands, enhance the sensitivity at the nanoscale by acting as signal generators or detectors [10]. Nanomaterials have unique advantages, including high reactivity, biological permeability, and multiplexing capabilities. Their properties, such as ultra-small size, high surface area-to-volume ratio, adjustable shape, intense signals, photosensitivity, and biocompatibility, allow for effective operation within the quantum-confined optical domain. Examples include noble metal nanoparticles (NPs), nanorods (NRs), quantum dots (QDs), up-conversion nanocrystals, and porous framework-based nanomaterials [11–13]. Their unprecedented controllability, stability, and multifunctionality have opened a new era in chemical and biological sensing, enabling rapid on-site detection with portable and cost-effective solutions. This review summarizes the fundamental mechanisms and key design principles for the assembly of optical sensors, with a focus on advanced nanomaterials that possess unique and essential properties. Additionally, the use of optical sensing in various biomedical and biopharmaceutical applications, such as *in vitro* diagnostics (IVDs), therapeutic drug monitoring, bioimaging, targeted therapy, and continuous drug monitoring using wearable or implantable devices, are summarized. The current limitations of these technologies are also discussed.

2. General principles of designing an optical molecular sensing platform for biomedical applications

An optical biosensor comprises two main components: a recognition system and a transducer platform. The recognition system determines the sensing performance characteristics, including sensitivity and specificity. The transducer platform converts the recognized events into optical signals. To achieve accurate sensing, two universal design strategies are summarized: the employment of reliable molecular recognition elements, and optimization of transducer platforms. Optical nanosensors can be divided into two primary categories based on the interaction mechanisms between the recognition element and targets: affinity and metabolism sensors [14,15]. Affinity sensors operate through binding interactions between a target and a receptor. Examples of these interactions include antigen-antibody binding, complementary DNA hybridization, and aptamer-based probes. The transducer platform generates optical signals in response to these complex formations. However, despite the prevalence of affinity sensors in the market, their progress is often limited by challenges such as inadequate recovery performance, as exemplified by disposable test strips. In contrast, metabolic or kinetic sensors, such as traditional glucose biosensors, use molecular recognition based on enzymatic reactions. These sensors facilitate the chemical conversion of the analytes into relevant visual products. Consequently, the content of the target analytes can be quantitatively determined using transducer platforms. These sensors offer several advantages, including reusability and portability, as the active enzymes demonstrate prolonged stability. In this section, the mechanisms and principles for constructing optical sensing platforms are introduced, considering the varying transduction of biorecognition events (Fig. 1). Moreover, recent developments in optical sensors for biomedical applications are also discussed.

2.1. Localized surface plasmon resonance (LSPR) for POC tests

Surface plasmon resonance (SPR) is a phenomenon in which conduction electrons on a metal surface are excited to oscillate collectively, coupled with electromagnetic waves due to light irradiation. This technique is effective for investigating the specific interaction modes between biomolecules, providing vital data such as kinetic parameters and affinity constants in a label-free and real-time manner [16]. In contrast to the SPR observed on individual substrates like thin metal films at the microscale, the plasmonic effect resulting from illuminating light on metal NPs at the

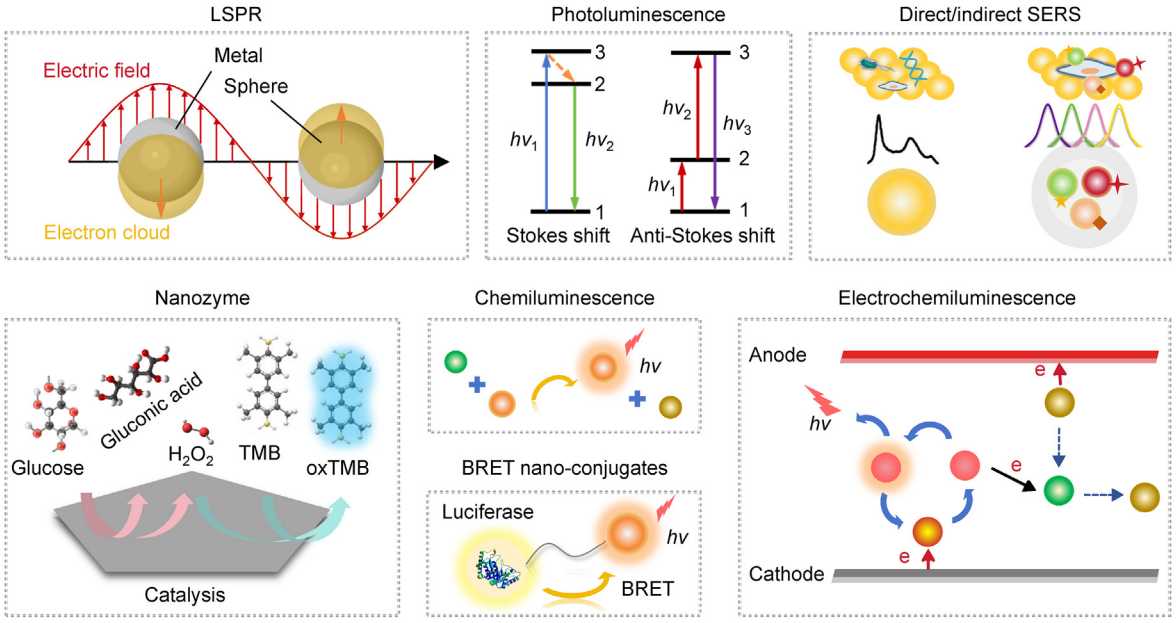

Fig. 1. Summary of the fundamental principles for nanomaterial-based optical biosensing. LSPR: localized surface plasmon resonance (SPR); SERS: surface enhancement Raman scattering; TMB: 3,3',5,5'-tetramethylbenzidine; BRET: bioluminescence resonance energy transfer.

nanoscale is referred to as LSPR. Noble metal NPs, particularly those composed of gold and silver, are electron-rich metals. They present extinction coefficients that are approximately 1000 times higher than those of most the organic dyes, owing to the LSPR effect. This electron-rich characteristic enhances their interaction with electromagnetic waves, leading to the effective excitation of surface plasmons. The formation of strong electromagnetic fields causes a Gaussian-like peak in the visible frequency range and a corresponding resonance occurs. The intensity and position of the LSPR peak substantially depend on several factors, including the size, shape, composition, surrounding dielectric medium, and the distance between adjacent nanostructures [17]. Therefore, target recognition processes can be conveniently identified by monitoring the shifts in the absorption band and corresponding color changes.

Typically, there are two LSPR sensing strategies based on the readout signals. The first strategy involves LSPR shift-based sensors that quantify recognition events based on spectral changes. The second strategy involves colorimetric sensors, which allow visual evaluation with the naked eye due to substantial absorption band shifts resulting from LSPR variation [17]. Spherical noble metal particles less than 50 nm in diameter exhibited a single resonance frequency. Consequently, conventional LSPR-based colorimetric platforms employ aggregation or disassembly mechanisms because interparticle plasmon coupling results in absorption band shifts of approximately 200 nm [18]. However, intensity or monochromatic changes limit the colorimetric quantification of the naked eye. In addition, non-response aggregation caused by environmental instability depresses the specificity and sensitivity. In response to these challenges, numerous plasmonic multicolorimetric sensors have been designed and proposed to achieve polychromatic transduction by adoption of the “non-aggregation” strategy. Considering the key factors influencing LSPR properties, the methods to achieve the most visible absorption spectrum coverage of LSPR variation resulting in a rainbow-like color change, can be summarized into two patterns: etching and growth-based mechanisms. Among the notable nanomaterials used in plasmonic multicolorimetric sensors are gold NRs (AuNRs), which are one-dimensional (1D) anisotropic NPs possessing at least two LSPR peaks. This property makes them unique for transducing morphological changes into a visible color change since the longitudinal band is particularly susceptible to their aspect ratio [19]. Herein, diverse noble metal nanomaterial-based etching and growth strategies have been proposed and applied to the assembly of multicolorimetric biosensors, especially for at-home blood and POC tests [20]. Proteins and antigens serve as important biomarkers for early diagnosis and prompt control of communicable and noncommunicable diseases, especially malignant tumors, acute cardiac dysfunction, and viral infections. In a conventional sandwich immunoassay system, a catalase-labeled antibody recognizes the target protein and subsequently translates the sensing reaction into a colorimetric readout. Unlike the monochromatic changes mediated by catalytic substrates, AuNR-etching-based multicolor immunoassays display vast vivid rainbow-like changes, allowing semi-quantitative visual detection [21]. Similar to AuNRs, Ag-shelled Au@AgNRs (AuNBP@Ag) exhibit marked optical properties during etching process. A multicolor sensor for squamous cell carcinoma antigen (SCCA) detection was developed based on catalase-mediated etching of AuNBP@Ag. The formation of a primary antibody-antigen-secondary antibody-sandwiched structure stimulates the catalysis of H_2O_2 to generate •OH, resulting in unusual longitudinal LSPR peak movements of the etched AuNBP@Ag. This colorimetric sensor achieved a linear detection of SCCA from 2.5 to 105 ng/mL, with a corresponding limit of detection (LOD) of 0.85 ng/mL with a spectrometer (Fig. 2A) [22]. Likewise, heteroepitaxial growth-mediated core-shell nanostructure formation also causes LSPR peak transitions and colorimetric variations. A facile and rapid enzymatic reaction-guided metallization colorimetric assay was developed based on Ag-deposition on the surface of AuNRs, achieving accurate measurement of β-galactosidase activity with a LOD of 128 pM. Combined with phage lysis, this assay was further optimized to detect infectious bacterial pathogens [23]. To improve the performance of LSPR sensors, Park and co-workers [24] demonstrated a binary mixture biosensing platform by integrating AuNRs and magnetically Pt@Ni nanorings to regulate plasmonic nanomaterials with an external magnetic field. This approach overcame the limitations of conventional designs such as core-shell NPs or multisegmented hybrid nanocomposites. Owing to its advantages including rapidity, accessibility, cost-effectiveness, portability, and simplicity, the lateral flow immunoassay (LFIA) is currently considered among the leading platforms for POC testing, particularly for at-home infection diagnosis and assessment. Chen and co-workers [25] achieved the ultrasensitive optical detection of hepatitis C virus antibodies in serum using a LFIA test strip. This was accomplished following the surface functionalization of a colloidal plasmonic core@magnetic shell nanocomposite by the co-assembly of Fe_3O_4 NPs and gold NPs (AuNPs) into polymer nanobeads. This enhanced plasmonic signal transducer provided at least a fourfold improvement in sensitivity. In addition, a dual-mode LFIA platform was also developed that utilizes the distinct optical properties of the Au-shelled AgNPs. This platform achieved simultaneous colorimetric and surface enhancement Raman scattering (SERS) detection of severe acute respiratory syndrome coronavirus 2 (SARS-CoV-2) IgG with the LOD of 10^{-7} mg/mL and 0.22 pg/mL in serum, respectively [26].

2.2. Fluorescence for biomedical diagnostics

Fluorescence is known as an established and dominant optical technique in biomedical diagnostics and real-time monitoring, even offering single-molecule detectable sensitivity and facilitating the real-time visualization of changes. When a fluorophore absorbs radiation at a different energy level, it emits fluorescent light at a specific wavelength. This process creates a wavelength difference referred to as the Stokes shift. In brief, there are two types of photoluminescence (PL) mechanisms: down-conversion and up-conversion. Fluorescent nanoprobes designed by both these processes have long been used in fluorescence-based optical biosensors [27]. Among these, NP-based fluorescent sensors have emerged as prominent devices with several distinct advantages, such as excellent photostability and biocompatibility, high emission rates, large Stokes shifts, and facile surface tailorability. Nevertheless, in traditional fluorescence-based optical biosensors, the intensity-based signal output can be inaccurate due to inconsistencies in instrumental parameters, background light scattering from sample matrices, and inadequate washout of nanomaterials. Recently, ratiometric fluorescent nanoprobes employing dual-emission strategies have gained considerable attention in biosensing applications, achieving greater discrimination convenience, higher sensitivity, and improved imaging contrast. The primary principles for designing ratiometric fluorescence-based biosensors can be classified into three categories. First, the close combination (at the nanoscale) of multiple fluorescent dyes with different emissions accomplishes dual-emission via Förster resonance energy transfer (FRET). These systems are defined as “two-dye-embedded NPs”. The second strategy involves choosing one nonluminous NP as a nanocarrier to conjugate two fluorescent dyes, where one fluorescent dye serves as a reference and the other responds to the target, referred to as “NP-dye nanoconjugates”. The final strategy involves the use of single or hybrid NPs with intrinsic dual emissions. The former type of NP

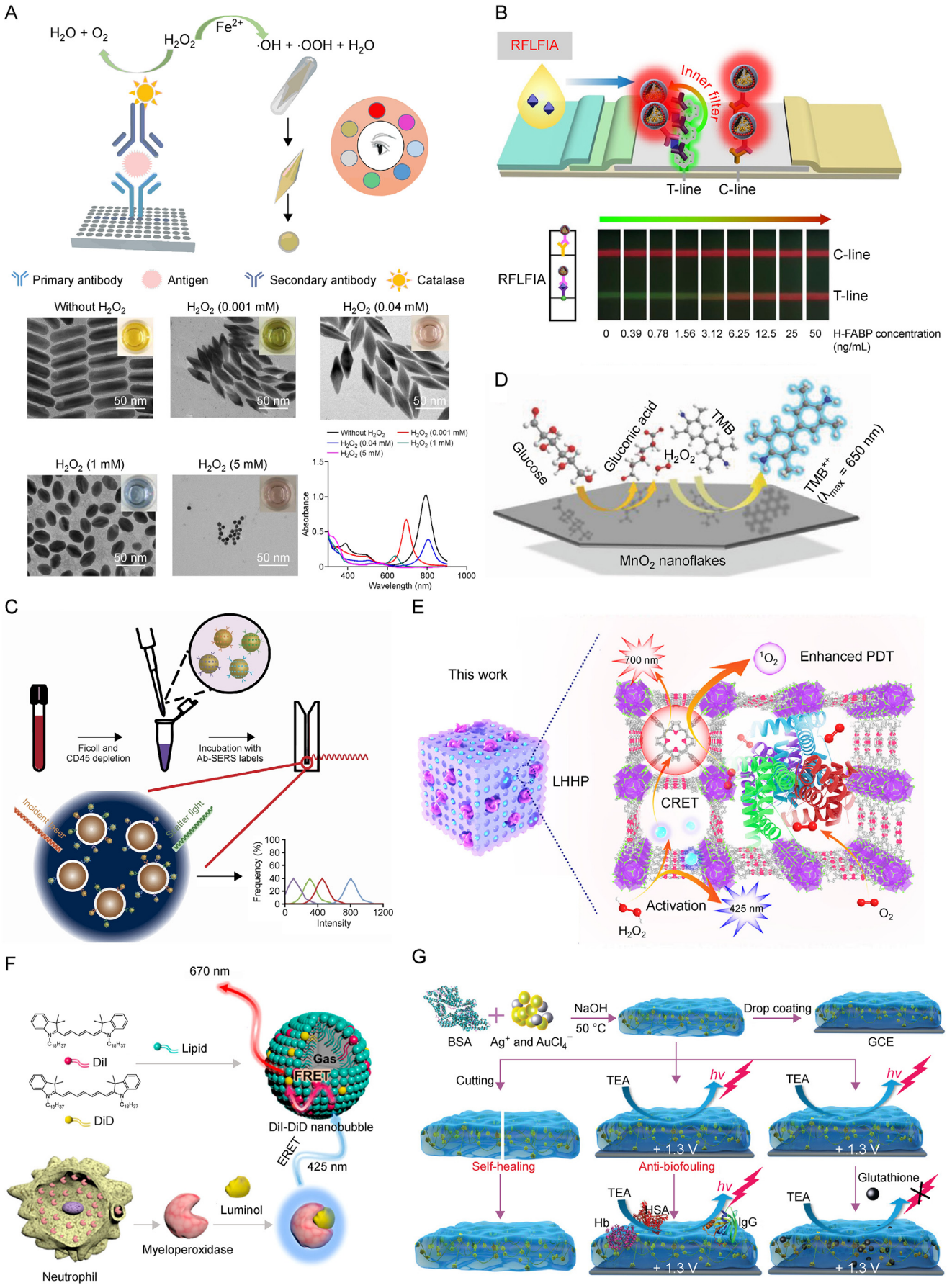
A
$H_2O + O_2$
H_2O_2
Fe^{2+}
·OH + ·OOH + H_2O
Primary antibody
Antigen
Secondary antibody
Catalase
Without H_2O_2
H_2O_2 (0.001 mM)
H_2O_2 (0.04 mM)
H_2O_2 (1 mM)
H_2O_2 (5 mM)
50 nm
Absorbance
Wavelength (nm)
B
RFLFIA
Inner filter
T-line
C-line
0 0.39 0.78 1.56 3.12 6.25 12.5 25 50
H-FABP concentration (ng/mL)
C
Ficoll and CD45 depletion
Incubation with Ab-SERS labels
Incident laser
Scatter light
Frequency (%)
Intensity
D
Glucose
Gluconic acid
H_2O_2
TMB
TMB^{*+} (λ_{max} = 650 nm)
MnO_2 nanoflakes
E
This work
LHHP
700 nm
$^1O_2$
Enhanced PDT
CRET
Activation
425 nm
H_2O_2
O_2
F
670 nm
DiI
DiD
Lipid
Gas
FRET
DiI-DiD nanobubble
ERET
425 nm
Luminol
Myeloperoxidase
Neutrophil
G
BSA
Ag^+ and $AuCl_4^-$
NaOH
50 °C
Drop coating
GCE
Cutting
TEA
hv
+ 1.3 V
Self-healing
Anti-biofouling
HSA
Hb
IgG
Glutathione

simplifies the ratiometric sensing design, whereas the latter retains the advantages of each element and enhances the operability for systematic integration [28]. To achieve a high visual resolution limited by traditional intensity-based color changes, a ratiometric fluorescence LFIA was proposed to detect heart-type fatty acid binding protein. This detection can be identified visually without aids or quantified using a smartphone. The combination of fluorescent silica nanospheres containing AuNPs, red-light-emitting CdSe/CdS/ZnS QDs as signaling reporters, and green-light-emitting CdZnSe/CdS/ZnS QDs as capture probes led to a target-induced color change from green to red. With the assistance of custom smartphone-dependent equipment, the detection limit was achieved at 0.21 ng/mL (Fig. 2B) [29]. However, a significant obstacle in achieving sufficient fluorescent signal quantity for the detection of various targets lies in energy transfer processes. An efficient and feasible strategy for avoiding FRET involves integrating tetrapod CdSe/CdS QDs with large Stokes shifts and a narrow full width at half maximum in conjunction with intrinsic CdSe/ZnS QDs. A conceptual $7 \times 7 - 1$ barcoding matrix and a 3D barcode library of 144 identifiable barcodes were constructed. These barcodes exhibited remarked multiplex sensing behavior for five common allergens towards specific IgE antibodies in the corresponding samples with a detection limit of 0.01–0.02 IU/mL [30]. In addition, a fluorescent visualization monitoring aptasensor based on a proximity-enhanced mechanism was demonstrated for efficient and multiple analysis of human epidermal growth factor receptor dimers on cell surfaces. The aptamer recognized protein targets and discriminated the expression states of homodimers and heterodimers by modulating the distance between two DNA-template Ag nanoclusters (AgNCs), resulting in the output of ratiometric signals [31]. Moreover, hybrid NPs with integrated plasmonic-fluorescent properties exhibited excellent performance in glucose sensing. In order to determinate the glucose and cholesterol levels in biological samples, photoluminescent biodots (Ser-Hist dots) and plasmonic AgNPs were combined to enable both fluorescent and colorimetric sensing. Under ultraviolet (UV) irradiation, Ag ions were anchored onto the biodots, leading to the spontaneous formation of AgNPs. This process displayed the plasmonic characteristics of the AgNPs and significantly quenched the signal intensity of biodots. Subsequently, the enzymatic oxidation of glucose or cholesterol resulted in an increase in H_2O_2 content, which stimulated the AgNP etching reaction, causing naked-eye distinguishable color changes and a simultaneous recovery of the biodots' fluorescent signal [32].

2.3. SERS spectroscopy for single-molecule analysis and circulating tumor cells (CTCs) detection

SERS spectroscopy is another nanoscale plasmonic phenomenon that enables the identification of the fingerprints of adsorbed targets and tracking alterations in surface chemistry [33]. The discovery of amplification and enhancement phenomena makes SERS competitive in optical biosensing, along with its remarked properties such as extremely high sensitivity, intrinsic structural specificity, and commendable experimental simplicity [34]. Notably, the enhancement of Raman scattering is closely related to the plasmon intensity, which is highly dependent on the gap distance. NPs such as Au nanowire (AuNW) vesicles provide large-volume "hot spots" and sharp tips as well as abundant gaps, which considerably intensify the signal [35]. The incorporation of revolutionary advancements in spectroscopic instrumentation, along with recent noteworthy developments in nanofabrication tools, has transformed SERS into feasible commercial biosensors rather than merely laboratory products. These techniques include lab-on-a-chip systems, endoscopic imaging, and microfluidics chips [36].

Direct and indirect approaches are the two most commonly employed schemes for SERS sensing. Direct SERS-based sensing represents the intrinsic SERS spectrum of a target in a straightforward manner, whereas indirect SERS strategies utilize the intensity and spectral profiles of Raman reporters to reflect alterations in recognition events [37]. Notably, significant advancements in nanopore-based DNA sequencing techniques have inspired technological renovations in fast and reliable single-molecule protein sequencing and structural analysis. However, the identification of 20 different amino acids, particularly non-aromatic amino acid residues, hinders further development in this field. Apart from the electrical readout method, optical detection methods such as SERS have shown potential in this field. By trapping sub-monolayer molecules adsorbed on Au nanostars (AuNSs) within an Au nanohole to form single strong hot spots, De Angelis and co-workers [38] firstly demonstrated distinct SERS spectroscopy with superior properties and distinguished 10 types of amino acids at the single-molecule level. Moreover, analysis of protein structures and conformational dynamics at physiological concentrations remains challenging. Dai et al. [39] developed a method that combines optical tweezers with Raman spectroscopy, utilizing two AgNP-coated silica microbeads to create tunable hotspots. This approach fulfilled ultrasensitive monitoring of flowing proteins in their native states and conformations.

In addition, SERS-based sensors have demonstrated potential for ultrasensitive CTCs sensing. Enumeration and analysis of the early stages of cancer have emerged as significant clinical platforms for cancer diagnosis and prognosis, *in vivo* drug resistance testing, and individualized treatments. However, the primary obstacle remains the highly effective and selective enrichment of CTCs from circulating blood. Consequently, several novel approaches have emerged for CTC detection, including immunomagnetic methods, size-based filtration techniques, and DNA-driven nanomaterial self-assemblies. Notably, the employment of NPs with different asymmetric shapes facilitates CTCs monitoring without the need for an enrichment process in biological samples. For example, three SERS-active NPs (AuNPs, AuNRs, and AuNSs) were functionalized with a Raman reporter molecule, reductive bovine serum albumin (BSA), and folic acid. This design achieved strong SERS signal output, high sensitivity, and excellent catching specificity, resulting

Fig. 2. Nanomaterial-enhanced optical biosensors and their biomedical applications: mechanisms based on varying transduction of biorecognition events. (A) Schematic illustration of the Ag-shelled Au@Ag nanorods (AuNBP@Ag)-based immunosensor and the etching process of the AuNBP@Ag in the absence and in the presence of different concentrations of H_2O_2. Insets are transmission electron microscopy (TEM) images. [22]. (B) Illustration of ratiometric fluorescent lateral flow immunoassay (RFLFIA) strip for visual and quantitative detection of heart-type fatty acid binding protein (H-FABP) [29]. (C) Circulating tumor cells (CTCs) detection by incubating with antibody-conjugated surface enhancement Raman scattering labels (Ab-SERS) and characterization with Raman spectroscopy [42]. (D) Nonenzymatic glucose colorimetric sensing based on MnO_2 nanoflakes. The $TMB^{\bullet+}$ indicate-soxidized TMB (blue product) [50]. (E) Schematic diagram of hierarchically porous porphyrinic metal-organic framework (MOF) to co-encapsulate luminol and hemoglobin for efficient chemiluminescence resonance energy transfer (CRET)-mediated and oxygen self-supply photodynamic therapy (PDT) of cancer [54]. (F) Schematic illustration of luminol + 1,1′-dioctadecyl-3,3,3′,3′-tetramethylindocarbocyanine perchlorate (DiI)-1,1′-dioctadecyl-3,3,3′,3′-tetramethylindodicarbocyanine perchlorate (DiD) nanobubbles for dual-modal imaging of myeloperoxidase activity through the bioluminescence resonance energy transfer (BRET), and the following Förster resonance energy transfer (FRET) between DiI and DiD [59]. (G) Schematic illustration of bovine serum albumin (BSA) directed fluorescent Au/Ag alloy nanoclusters (Au/AgNCs@BSA) hydrogel-based electrochemiluminescence sensing system for glutathione detection [61]. TMB: 3,3',5,5'-tetramethylbenzidine; LHHP: luminol and hemoglobin co-encapsulated hierarchically porous porphyrinic MOF; GCE: glassy carbon electrode; TEA: triethylamine; Hb: hemoglobin; HSA: human serum protein. Reproduced from Refs. [22,29,42,50,54,59,61] with permission.

in an enhanced LOD of 1 cell/mL [40]. Besides, SERS-based technologies have extraordinary potential for separating and analyzing the diverse molecular characteristics of CTCs in real-time. Cui and co-workers [41] reported a size-based microfluidic cell isolation assisted on-chip SERS strategy for real-time monitoring of cell membrane proteins and malignancy classification. A SERS vector was constructed by integrating spherical AuNPs, a thin silver shell, Raman reporters, and DNA aptamers. Additionally, three spectrally orthogonal SERS-based aptamer nanovectors systems were assembled, achieving a good classification performance with high sensitivity and accuracy for various cancer cells. Real-time monitoring of the phenotypic evolution of CTCs during therapeutic processes is important for treatment management. Tsao et al. [42] proposed a multiple CTC surface markers characterization strategy based on antibody-conjugated and Raman reporter-coated AuNPs multiplex SERS nanotags. This approach allowed simultaneous profiling and evolutional monitoring of CTCs during melanoma treatment (Fig. 2C) [42]. This sensor exhibited exceptional sensitivity for CTC detection by identifying 10 cells in 10 mL of blood without the need for isolation. It also responds accurately to tumor cell populations during targeted treatment. Using this strategy, different CTC signatures of underlying clinical significance in drug-resistant clones were observed.

2.4. Nanozyme for biologically related molecules detection

In 2007, the identification of Fe_3O_4 NPs exhibiting peroxidase-like activities simulated the emergence of numerous enzyme mimics especially "nanozymes" [43]. Nanomaterials have presented extraordinary properties in catalyzing peroxidase substrates such as 3,3',5,5'-tetramethylbenzidine (TMB), diazoaminobenzene, and *o*-phenylenediamine, leading a detectable color changes due to the oxidization of the substrates in the presence of H_2O_2. These properties have been exploited for the optical sensing of glucose, xanthine, and cholesterol [44–46]. As one of the global health issues, diabetes affects a considerable portion of the population, and its management heavily relies on continuous monitoring of blood glucose levels with high accuracy. Currently, optical enzymatic sensors based on glucose oxidation are commonly used to track body glucose levels [47]. Inspired by natural enzymes, nanozymes are generally applied as a potential alternatives because of their cost-effectiveness, stability, and mass-producibility. To overcome challenges related to low diffusion efficiency and unstable intermediates, integrated nanozymes composed of low-dimensional nanomaterials have been widely developed. An innovative hybrid nanosheet was fabricated for the colorimetric measurement of glucose, achieving a detection limit reaching 8.5 mM. This biomimetic catalyst consists of ultrasmall AuNPs and 2D metalloporphyrinic metal-organic framework (MOF) nanosheets, in which the AuNPs serve as artificial glucose oxidase, while the metalloporphyrinic MOF nanosheets function as nanozymes. These hybrid nanosheets were prepared using TCPP(M) (TCPP = tetrakis(4-carboxyphenyl)porphyrin, M = Fe, Co) as ligands and $Cu_2(COO)_4$ paddle-wheel clusters as metal nodes with further growth of AuNPs, and exhibited potential for use as novel artificial enzymes in bioassays and nanomedicines [48]. Moreover, AuNPs were further modified with cyclodextrin, resulting in the construction of macrocycle-AuNP hybrid nanomaterials. Regularly arranged 1D and 2D architectures provide versatile nanoplatforms for detection, self-assembly, and sequential catalysis. Notably, a cascade reaction for glucose sensing was successfully achieved since the proposed nanomaterials demonstrated distinct catalytic activities comparable to those of glucose oxidase and horseradish peroxidase (HRP) [49]. Han et al. [50] also demonstrated BSA-directed MnO_2 nanoflakes exhibiting cascade enzyme-like properties for colorimetric detection of glucose. The single nanozyme simultaneously oxidized glucose and allowed the optical measurement of H_2O_2 levels (Fig. 2D) [50].

2.5. Chemiluminescence and bioluminescence for in vivo sensing and imaging

In vivo bioimaging techniques possess outstanding capabilities for probing active biological specimens and revealing cell damage or dysfunction associated with serious diseases. Chemiluminescence refers to the emission of light resulting from chemiexcitation during a chemical reaction [51]. Unlike fluorescence-based techniques, which are hindered by fluorescence quenching and poor tissue penetration, chemiluminescence-base sensors eliminate the need for external light excitation and reduce background autofluorescence interference. This results in higher sensitivity detection and deeper tissue imaging with an extremely high signal-to-noise ratio. As an application, a noninvasive strategy for detecting both exogenous and endogenous hypochlorite was developed using a glow-type chemiluminescent probe. This probe was further applied to investigate the physiological and pathological roles of hypochlorite *in vivo* [52]. In contrast to direct chemiluminescence processes, indirect chemiluminescence methods, such as chemiluminescence resonance energy transfer (CRET), involve an energy transfer process from an excited state intermediate to adjacent fluorescent molecules or nanomaterials, which then trigger light emission. Recently, improved nanomaterials, including QDs, metal/metal oxide NPs, mesoporous silica nanomaterials, and MOFs have been introduced to optimize chemiluminescence sensing and imaging using the CRET strategy [53]. A novel all-in-one CRET-based chemiluminescence photodynamic therapy (PDT) platform was developed by combining hemoglobin and luminol with MOFs. The porphyrinic photosensitizing linker, TCPP, was well dispersed in the framework nanophotosensitizer with the co-encapsulation of luminol and hemoglobin. Upon exposure to elevated levels of H_2O_2 in the tumor microenvironment, luminol generated blue chemiluminescence. Subsequently, the emitted light is absorbed by the TCPP components within the MOF NPs via the CRET mechanism, resulting in luminescence emission. The excited-state energy is then transferred to oxygen molecules bound by hemoglobin, leading to the production of cytotoxic reactive oxygen species (ROS). This platform allows simultaneous *in situ* imaging and therapy simultaneously through H_2O_2-activated CRET and subsequent oxygen self-supply (Fig. 2E) [54].

Bioluminescence was initially explored as a natural light-emitting phenomenon in cells or animals in 1667. It has since evolved into an advanced autofluorescence-free optical imaging technique for highly sensitive visualization that relies on the catalytic reaction between luciferase enzymes and a small-molecule luciferin analog to form an excited-state species [55]. However, the light emitted by some natural luciferins, such as coelenterazine, is intensively absorbed by blood or tissue, which presents limitations for *in vivo* imaging [56]. Thus, bioluminescence resonance energy transfer (BRET) nanoconjugates have been developed as effective solutions to overcome these challenges. Fluorescent nanomaterials, such as QDs or quantum rods (QRs), are perfectly competent to function as BRET acceptors because of their excellent brightness, large Stokes shift, and narrow/tunable emission. Notably, the covalent conjugation of NanoLuc luciferase to silver sulfide QDs generates near-infrared II (NIR-II) photons, shifting bioluminescence based on the reaction with luciferin substrate and a single-step BRET process. This innovation has enabled deep tumor *in vivo* imaging with considerably excellent signal-to-noise ratios and sensitivity while remaining nontoxic for NIR-II emission [57].

Moreover, recent findings indicate that BRET ratios are highly responsive to aspect ratios when utilizing QRs as acceptors. The QR-luciferase nanoconjugates featuring short rods exhibiting long-wavelength emissions display the highest efficiency [58]. The integration of BRET and FRET processes represents another effective strategy for enhancing the tissue penetration and spatial resolution of luminol-based biomarker-targeted imaging. Accurate *in vivo* evaluation of the inflammation-related biomarker, heme-containing enzyme myeloperoxidase, is essential for the early diagnosis and surveillance of the progression in inflammatory disorders, including Alzheimer's disease and cancer. A lipid nanobubble fabricated by Liu et al. [59] incorporated two tandem lipophilic dyes to redshift luminol-emitted blue light to NIR region by an integrated transversion of BRET-FRET. This approach achieved bioluminescence/ultrasound dual-modal enhanced myeloperoxidase-dependent inflammation imaging within a breast cancer animal model (Fig. 2F) [59].

2.6. Electrochemiluminescence for bioanalytical detection

Electrochemiluminescence is an attractive signal generation strategy that involves the conversion of electrical energy into radiative energy without requiring external light sources. This occurs when the species generated at the electrodes emit light as a result of undergoing energy-intensive electron-transfer processes that lead to the formation of excited states. This method merges the principles of electrochemistry and spectroscopy, capitalizing on the benefits of both disciplines. Electrochemiluminescence technology offers considerable advantages for bioanalytical detection, including miniaturization, low background noise, cost-effectiveness, high sensitivity, and rapid response. Electrochemiluminescence is typically generated via two primary mechanisms: annihilation and coreactant pathways. Compared with the annihilation pathway, the coreactant pathway exhibits improved stability against radical ions in aqueous environments, higher electrochemiluminescence intensity, and broader applicability, enhancing its suitability for practical use. Regardless of the different electrochemiluminescence mechanisms, most electrochemiluminescence processes typically involve four main stages: redox reactions at the electrode surface, homogeneous chemical reactions in solution, formation of excited-state species, and emission of light [60]. Five primary types of electrochemiluminescence sensing strategies are categorized. Compared with the most traditional approach involving direct use of an electrochemiluminescence emitter as a signal label, the prevalent method utilizes the spatial hindrance or resistance effects resulting from bio-recognition events. A convenient strategy is to leverage the interactions between analytes and electrochemiluminescence substances like luminophores or excited-state electrochemiluminescence molecules, while the fourth approach focuses on the interaction between analytes and coreactants. The most sophisticated method involves modulating electrochemiluminescence light emission, predominantly through an emerging technique known as electrochemiluminescence resonance energy transfer (ECL-RET). This approach capitalizes on the intrinsic sensitivity of ECL-RET at the nanoscale and the diverse potential of nanomaterials as donors or acceptors. Consequently, this innovative strategy offers substantial opportunities for enhancing electrochemiluminescence sensing applications by utilizing the distinctive characteristics of nanomaterials. In addition to employing a target-specific molecular recognition functionalized working electrode, which is similar to most electrochemical assays, the applied potential in electrochemiluminescence systems generates luminescent signals by exciting the electrochemiluminescence probe. Han and Guo [61] demonstrated a hydrogel-based system incorporating fluorescent Au/AgNCs to eliminate nonspecific interferences and physical damage to the electrochemiluminescence sensing interfaces. This approach achieved a detection limit of 8.7×10^{-6} M for glutathione sensing in serum (Fig. 2G) [61]. In that study, the fluorescent Au/AgNCs served as highly effective electrochemiluminescence probes in a hydrophilic hydrogel matrix. These NCs underwent electro-oxidation near the electrode surface to form Au/AgNC^{+} species. The subsequent reaction with reductive radicals (produced by the electro-oxidation and deprotonation of the co-reagent) led to the formation of an excited state in the NCs, thereby inducing light emission. In recent years, significant progress has been made in the development of electrochemiluminescence-based biosensors for rapid and high-throughput monitoring of drugs related to physiological functions. An enzyme-functionalized single microbead-based imaging strategy was developed for the determination of lecithin by utilizing a luminol derivative and H_2O_2. The resulting electrochemiluminescence signal was captured and imaged using a camera, which enabled precise quantitative analysis with a LOD of 0.05 mM. Despite the heterogeneity observed in individual gold microbeads, their luminescence adheres to statistical consistency [62].

3. Key nanomaterials for optical sensing in biomedical and biopharmaceutical research

Materials characterized by particle sizes reduced to the nanoscale regime exhibit significantly enhanced mechanical properties and have become promising candidates for high-performance sensors components. Fig. 3 provides a comprehensive comparison of key nanomaterials for optical biosensors, categorized into 0D, 1D, 2D, and 3D nanomaterials. 1D materials are related to the structures with two of the three dimensions below 100 nm, whereas 2D materials exhibit a sheet-like architecture with a horizontal dimension exceeding 100 nm [63,64]. Similar to their 0D counterparts such as NPs and metal/carbon compound QDs, 2D nanostructures, including nanosheets, transition metal dichalcogenides (TMD), and transition metal carbides/carbonitrides (MXenes), also exhibit exceptional optical properties as fluorophores, nanoquenchers, or nanozymes [65,66]. Moreover, the unique geometrical characteristics of 1D nanostructures, such as NRs, make them particularly desirable for multicolorimetric sensing [22]. In addition, 3D nanomaterials, especially porous framework-based nanomaterials and nanodiamonds, hold great potential in multiple applications, including drug delivery, gas storage and extraction, photonics, and catalysis [65,67].

3.1. 0D nanomaterials for IVDs and therapeutic drug monitoring

3.1.1. Noble metal nanomaterials

Precise *in vitro* optical diagnostic and therapeutic drug monitoring techniques have substantial value in medical profession and at-home healthcare to make clinical diagnosis rapid, straightforward, easy, and less painful. These advancements have also guided personalized medicine, continuous monitoring, and targeted therapies in their early stages. Typically, currently available IVD systems are developed to precisely detect individual biological circulating targets, including proteins, nucleic acids, whole cells, metabolites, and drug molecules. These targets provide real-time feedback of patients' physiological and pathological conditions. The integration of numerous low-dimensional nanomaterials with superior features has propelled the development of IVDs into a new era towards precision medicine. Currently, 0D materials being extensively explored primarily include noble metal NPs/NCs, metal oxide NPs, semiconductor QDs, nanocarbons, and up-conversion NPs. These materials have promising prospects for IVDs and drug monitoring, owing to their diverse synthesis methods and multiple quantum properties. Noble metal NPs, including Au, Ag, and Cu exhibit

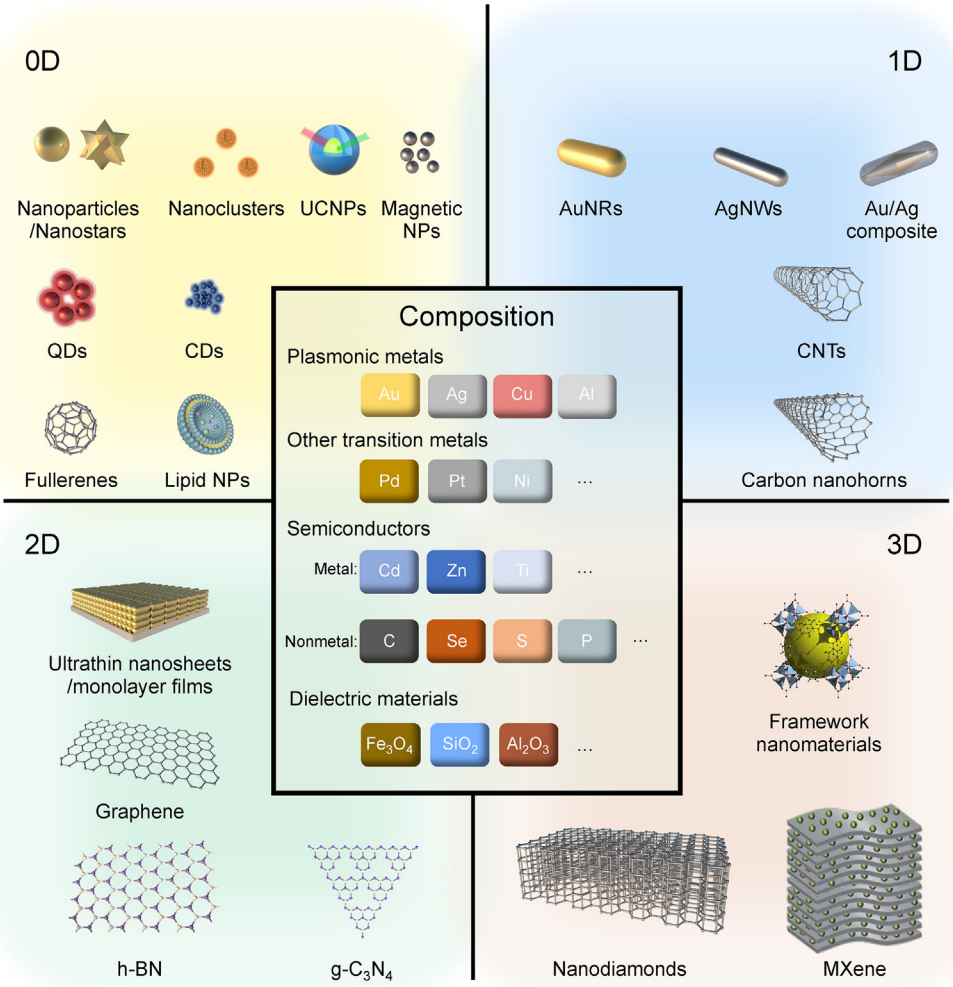

Fig. 3. Comparison of key nanomaterials for optical biosensors, classified according to the categories of zero-dimensional (0D), 1D, 2D, and 3D nanomaterials. UCNPs: upconversion nanoparticles (UCNPs); NPs: nanoparticles; QDs: quantum dots; CDs: carbon dots; AuNRs: gold nanorods; AgNWs: silver nanowires; CNTs: carbon nanotubes; h-BN: hexagonal boron nitride; g-C_3N_4: graphitic carbon nitride.

attractive LSPR properties and their performance is significantly influenced by their shape and size. The aggregation mechanism of large metal spherical particles below 50 nm such as AuNPs and AgNPs is typically utilized in monochrome colorimetric sensing platforms, where the formation of nearby plasmon couplings leads to noticeable color changes [68]. Besides, noble metal NPs particularly AuNPs have been regarded as promising candidates for SERS biosensing platforms, enhancing the Raman scattering capacity of the absorbed species and enabling spectroscopic identification, even at the single-molecule level. Based on this sensing principle, a sandwich-type SERS biosensor was prepared to detect miR-141 with ultra-high sensitivity at the femtomolar level using a multiple-signal magnification scheme. In particular, giant AuNWs achieved initial signal enlargement by the advantage of large-volume hot spots, while silver stain, signaling molecule R6G and hybridization chain reaction (HCR), as well as the Fe_3O_4@AuNPs capture units further facilitated the sensing performance [35]. A clustered regularly interspaced short palindromic repeat (CRISPR)-Cas12a-assisted SERS sensor was also established for the ultrasensitive diagnosis of various viral nucleic acids, including those of the hepatitis B virus, human papillomavirus 16 (*HPV*-16), and *HPV*-18. In this platform, a nanoarray was functionalized with graphene oxide (GO) and trianglar Au nanoflowers. The Raman probe-integrated AuNPs significantly enhanced the output signals, achieving a sensitive LOD of 1 aM [69]. The development of therapeutic drug monitoring techniques has laid the foundation for an era of "personalized medicine", enabling the customization of treatments based on individual genetics, lifestyle, and environmental influences. Continuous drug monitoring provides real-time feedback, facilitating timely adjustments to treatment dosages, particularly for medication with substantial side effects, such as doxorubicin. To achieve rapid and cost-effective detection, Quarta et al. [70] developed a plasmonic biosensor utilizing gold nanoislands partially embedded in a glass substrate and subsequently coated with Al_2O_3 to form Au/Al_2O_3 core-shell structures. The LSPR-based detection of doxorubicin relied on a concentration-dependent red-shift peak, achieving LODs of 1 nM in water and 16 nM in both bovine and human serum. By modifying the nanoislands with Al_2O_3, SERS measurements exhibited enhanced sensitivity due to the electronic and energy interactions between adjacent Au nanoislands and between doxorubicin molecules and gold. This method achieved a low LODs of 100 pM in water and

1 nM in fetal bovine serum. Au@Ag core-shell NPs also generated abundant 3D hotspots on the superhydrophobic self-assembled AgNP film, even with the interference from the complex plasma matrix. The proposed silver-film-assisted 3D SERS sensor achieved the measurement of crystal violet at concentrations as low as 10^{-13} M and facilitated the pharmacokinetics investigation of mitoxantrone and methylene blue following intravenous injection in mice through blood collection [71]. In addition to blood and serum samples, the dermal interstitial fluid shows substantial potential for *in vivo* drug monitoring. A SERS-based microneedle array was developed by integrating core-satellite organized Au@AgNPs and hydrogel-coated microneedles, enabling the non-invasive and *in situ* analysis of methylene blue and mitoxantrone. Furthermore, results from a drug-injected mouse model demonstrated that the mitoxantrone level within the skin's interstitial fluid was significantly lower than that in the blood, whereas the concentrations of mitoxantrone were comparable [72]. Aminoglycosides, which belong to a category of antibiotics, are frequently used in addressing infections resulting from gram-negative bacteria, such as tuberculosis. Owing to their negative side effects, it is imperative for drug monitoring to ensure safe and effective individualized dosing regimens. A high-throughput biosensor capable of dual detection of aminoglycoside antibiotics using both LSPR and SERS was developed on a single platform, leveraging the aggregation phenomenon of AuNPs induced by surface charge interactions with antibiotics. Although this sensing approach has demonstrated the feasibility of detecting tobramycin, the use of NPs in physiological fluids can lead to inaccurate measurements owing to the formation of a protein corona, resulting in poor repeatability and reduced accuracy. Therefore, essential modifications are frequently necessary to prevent the self-aggregation of 0D metal NPs, thereby limiting their practicality and availability [73]. The SERS-based platform also demonstrated superior capabilities for the real-time monitoring of both the depth of penetration and drug release kinetics of NIR light-responsive nanomedicine *in vivo*. The temperature increase of the waxberry-like AuNPs triggered the release of curcumin, leading to a corresponding decrease in the SERS intensity. This reduction in SERS intensity also accurately reflected the penetration depth of the nanomedicine within the tumor [74].

When the size of metallic particles is smaller than that of the electron mean path, these particles exhibit weak fluorescence emission called NCs. Notably, NCs with ultra-small sizes (<2 nm) present distinct crystal structures and exhibit fluorescence properties, whereas the previous unique LSPR phenomenon disappears. There are two typical strategies for preparing metal NCs, i.e., the reduction of metal precursors and the etching of larger nanomaterials with the assistance of robust stabilizers. The novel intrinsic dual-emissions optical properties of these NCs further expand their biomedical and biopharmaceutical applications in optical sensing, biolabeling, and bioimaging. Hairpin DNA-templated AgNCs represent a novel type of chameleon nanomaterial with two emission peaks. The intensities of these peaks can be inversely regulated through the hybridization of target DNA on the loop segment, which increases the distance between the two emitters. Based on this strategy, our research group reported a dual-emitter DNA-AgNCs-based ratiometric fluorescent sensor for single-nucleotide polymorphisms (SNPs) discrimination with high accuracy and sensitivity. This optical sensing platform identified various types of SNPs by introducing a peptide nucleic acid clamp and an isothermal amplification reaction. The mismatch of the nucleic acid base pair led to a color shift from red to green, which was easily distinguished by the naked eye [75]. Specifically, the discrimination capacity of this sensor was sufficiently presented through vivid color changes due to the enlargement of the Ag emitter pair, resulting in a substantial reduction in red emission and the subsequent appearance of green emission under UV light stimulation. Moreover, noble metal-based nanomaterials are also promising candidates for therapeutic drug delivery. A multifunctional theranostic nanosystem based on nanocarrier AuNCs was developed to deliver platinum (IV) drugs, featuring NIR-II imaging capability and intracellular glutathione scavenging activity. Inhibition of tumor growth was further validated using two malignant tumor models (Fig. 4A) [76]. However, the sensitivity of NCs to varying sensing conditions, such as pH and temperature, and their tendency to form non-reversible aggregates complicate their functionalization and storage [77]. Moreover, the controlled preparation of NCs remains poorly understood, as most methods have been developed through trial and error. Therefore, a more comprehensive insight into the diverse aspects of NC synthesis and their interactions with target molecules will advance the rational design of materials. On the other hand, many noble metal nanomaterials, including Au, Ag, Pt, Pd, and their multimetallic NPs, exhibit peroxidase-mimicking properties and have been extensively applied in IVD. Li et al. [78] synthesized an innovative Cu@Zr nanozyme using a self-assembly process that simultaneously displayed attractive enzymatic and fluorescence properties. The cascade catalytic reaction induced by Cu@Zr led to the production of a red quinoneimine, facilitating the colorimetric detection of urease, which was further enhanced by urea hydrolysis. Meanwhile, the fluorescence signals of Cu@Zr gradually decreased due to the accumulation of red quinoneimine, achieving a swab-based dual-mode sensor for real-time identification of urease with the assistance of a smartphone. Active thiol-containing stabilizers, such as *N*-acetyl-L-cysteine (NAC), possess a high affinity for metal ions and improve the catalytic performance of noble-metal nanozymes. A NAC-PtNCs functionalized sensing platform was proposed to quantitative identification of heparin by catalyzing TMB substrate to produce detectable signals, achieving a LOD of 2×10^{-3} μg/mL in heparin spiked human serum samples [79]. This biosensor facilitates the provision of information and guidance regarding medication dosage for both intraoperative and postoperative clinical procedures. Additionally, it helps prevent serious complications arising from excessive dosage or prolonged use, such as hemorrhage, thrombocytopenia, and osteoporosis.

3.1.2. Metal oxide nanomaterials

To avoid the excessive costs associated with high-priced noble metals, researchers have begun to exploit the value of cost-effective and accessible oxide materials such as Cu_2O, Fe_2O_3/Fe_3O_4, Co_3O_4, CeO_2, and MnO_2 [80]. Iron oxide-based magnetic NPs possess distinct intrinsic peroxidase-mimicking properties and that were first reported in 2007 [43]. Since then, iron oxide-based peroxidase mimics have been extensively investigated, including Fe_3O_4, Fe_2O_3, doped ferrites, and relative compositions. A nanozyme synthesized by integrating $CoFe_2O_4$ with porous carbon demonstrated superior peroxidase mimetic activity compared with that of each individual component, and was employed to detect glucose and glutathione [81]. Additionally, copper containing oxide NPs, such as Cu_2O/polypyrrole composites and molybdenum trioxide NPs, have been widely established as oxidase mimics, whereas Co_3O_4 and ZrO_2 primarily exhibit catalase-mimicking activities at high pH [82,83]. In addition, a variety of oxide nanostructures with different morphologies, including octahedral Ag_2O, ZnO nanosheets, TiO_2 nanostructures, Cu_2O superstructures, SnO_2 NPs, $W_{18}O_{19}$ NWs, and Ta_2O_5 NRs, have garnered substantial interest because of their remarkable characteristics as catalysts and SERS-active probes [84–86]. The excellent biocompatibility, spectral stability, and sensitivity of these oxide nanostructures make them promising candidates for cancer cell diagnosis and imaging. To address the substantial challenge posed by the extreme rarity of CTCs in

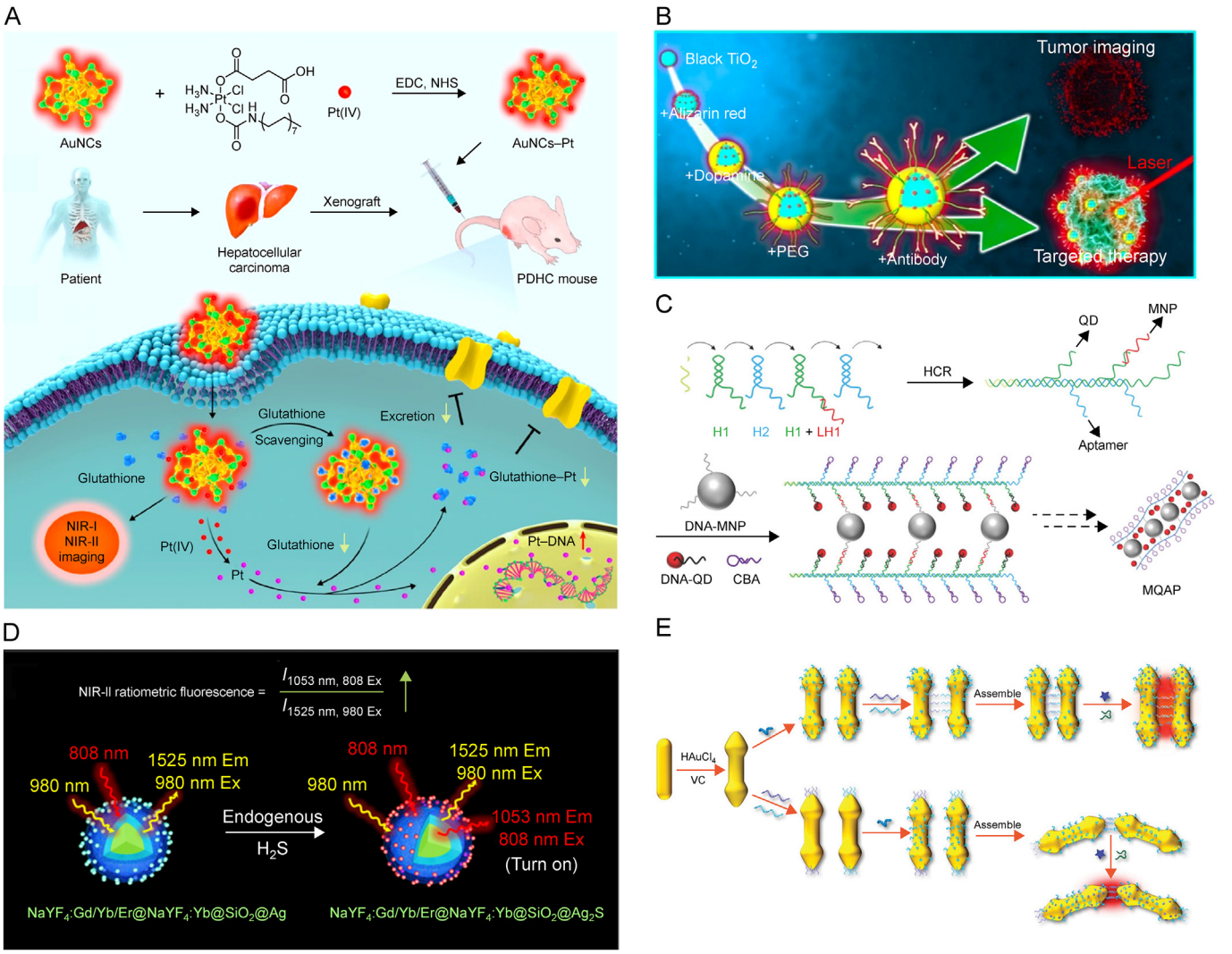

Fig. 4. Zero-dimensional (0D) and 1D nanomaterials for *in vitro* diagnostics (IVDs) and therapeutic drug monitoring. (A) Synthesis illustration of the platinum (IV) delivered gold nanoclusters (AuNCs−Pt) and the corresponding near-infrared II (NIR-II) tumor imaging capacity penetrates deep tissues, allowing visualization of the platinum transportation [76]. (B) Schematic diagram of the design process for black TiO_2 (B−TiO_2) bioprobe and its application in biological surface enhancement Raman scattering (SERS) imaging and photothermal therapy [85]. (C) Schematic illustration of DNA-templated magnetic nanoparticle (NP)-quantum dot (QD)-aptamer copolymers (MQAPs) for magnetic isolation of circulating tumor cells (CTCs) [88]. (D) Schematic design of activatable orthogonal NIR-II emitting $NaYF_4$:Gd/Yb/Er@$NaYF_4$:Yb@SiO_2@Ag nanoprobes for hepatotoxicity detection induced by overdose metformin [97]. (E) Scheme of DNA-bridged arrowhead gold nanorod (AuNR) dimers with side-by-side and end-to-end motifs for miR-21 detection in living cells [104]. EDC: *N*-(3-dimethylaminopropyl)-*N*′-ethylcarbodiimide hydrochloride; NHS: *N*-hydroxysuccinimide; PDHC: a patient-derived tumor xenograft model of hepatocellular carcinoma; PEG: polyethylene glycol; HCR: hybridization chain reaction; MNP: magnetic NP; CBA: a DNA aptamer (sgc8c); MQAP: DNA-templated MNP-QD-aptamer copolymers; VC: vitamin C. Reproduced from Refs. [76,85,88,97,104] with permission.

peripheral blood, an octahedral Ag_2O NPs-based sensing platform was developed. This platform exhibited notable SERS with an ultra-high enhancement factor (EF) of 1.98×10^6 for 4-mercaptopyridine molecules. The synergistic effects of the surface defect-enhanced photo-induced charge transfer and robust vibrational coupling resonance within the Ag_2O-molecule SERS complex significantly amplified the molecular Raman scattering cross-section. After modification with folic acid via an amide bond linkage, this bioprobe achieved a LOD of 1 cell/mL for CTCs in blood samples [84]. In addition, antibody-fabricated crystalline core-shell structured black TiO_2 NPs with positive SERS activity were synthesized to develop a bioanalytical strategy for targeting and monitoring MCF-7 cells with drug resistance (Fig. 4B) [85]. Owing to the highly efficient exciton transfer within the crystalline core and the band bending at the interface of the crystal-amorphous heterojunction, sufficient photoinduced charges were generated, enabling efficient exciton dissociation and charge transfer. This led to the accumulation of photoinduced charges in the amorphous shell, thereby facilitating efficient interfacial photoinduced charge transfer between the substrate and target molecules. Furthermore, this platform was particularly advantageous because of its additional photothermal therapeutic properties under 808 nm laser irradiation, and black TiO_2 NPs could be also considered as an effective nano-drug. Thus, intelligent theragnostic nanosystems that integrate diagnostic and therapeutic functions have emerged as techniques for early intervention and effective control of cancer. Overall, the biocompatibility, versatility, and resource sufficiency of metal oxides have significantly accelerated their progression in IVDs and therapeutic drug monitoring. However, when developed as an integrated diagnostic and therapeutic nano-drug, the biological toxicity and metabolic characteristics of metal oxide nanomaterials require comprehensive investigation.

3.1.3. Semiconductor QDs

Fluorescent QDs are typically made from semiconducting NPs, particularly metal chalcogenide QDs such as CdSe- and CdTe-based QDs which have gained considerable attention owing to their advantageous photonic quantum effects and higher fluorescence quantum yields compared with those of upconversion NPs (UCNPs) [87]. DNA molecules have also demonstrated their potential as precise recognition and nanomaterial self-assembly. By utilizing a CTC-binding aptamer (sgc8c) and HCR, a novel QD-based copolymers were synthesized for trackable magnetic separation of CTCs from blood samples, achieving a high capture efficiency and purity of nearly 80%. The DNA-CdTe/CdS core/shell QDs featured an excellent quantum yield of 41.8%, and these inorganic magneto-fluorescent materials were able to penetrate cells (Fig. 4C) [88]. Similarly, a facile all-nucleic-acid assisted amplification-based QDs reporter was developed for consistent visual and fluorescent detection of A549 lung cancer cells in blood samples. When recognizing mucin 1 or A549 cells, the aptamer is released from the dsDNA probe and triggers catalyzed hairpin assembly-based amplification. Concurrently, the CdTe QDs specifically recognized the unbound Ag^+ from C—Ag^+—C structures to produce visualized fluorescent responses, achieving a LOD of 0.15 fg/mL (mucin 1) and 3 cells/mL (A549 cells) [89]. Among all the DNA-driven nano-assembly-based sensing methods, fluorescence quenching and metal-enhanced fluorescence (MEF) effects have been widely proposed owing to their rapid response times, intense optical activity, and multiplex targeting capabilities. Numerous sensing platforms have been constructed based on the regulated distance between the metallic material and the fluorescent signaling probe, as the fluorescence quenching phenomenon can be manipulated. Nevertheless, when the fluorescent probe is positioned within 10 nm of the noble metal nanostructures, the fluorescence signal is enhanced due to the LSPR of noble metal particles upon exposure to incident light. Based on the MEF effect, precise determination of the prostate cancer marker PCA3 sequence was achieved by regulating the distance between AuNRs and NIR Ag_2S QDs using DNA with various chain lengths [90]. Some essential amino acids, such as cysteine, play a critical role in maintaining intracellular redox balance to sustain the equilibrium between free thiols and oxidized disulfides. Plasma cysteine levels are strongly associated with various diseases. A rapid-response optical biosensor for cysteine determination was developed based on nitrogen-doped graphene QDs (N-GQDs) with vanadium pentoxide nanosheets, which function as fluorescence turn-off/on nanoprobes. In this system, the V_2O_5 nanosheets act as both fluorescence quenchers and as target recognizers. Specifically, the detection of cysteine initiated the reduction of V_2O_5 to V^{4+} and the release of N-GQDs, leading to a fluorescence response and achieving a LOD of 50 nM with high selectivity [91]. Moreover, immunohistochemistry-based bioimaging techniques are highly suitable for *in situ* single-cell immunoprofiling and can provide comprehensive information about intracellular protein expression owing to the widespread accessibility of specific antibodies and well-established approaches for fluorophore biological conjugation. The combination of QDs and amplification reactions allows sensitive and multiplexed protein analysis at the single-cell level. Five to ten QD colors can be simultaneously labeled to target antigens using a signal amplification procedure without negatively affecting sample antigenicity [92].

However, the application of flammable and toxic dimethylcadmium has restricted the practicality of QDs. Therefore, extensive efforts have been made to enhance synthesis methods using various stable and safer precursors (e.g., CdO, SeO_2, and $Cd(OOCR)_2$), non-coordinating solvents, and stabilizers [93]. Additionally, passivation and toxicity reduction of fluorescent QDs have been accomplished by coating them with inert shells and performing surface modifications [94]. Notably, when wide-bandgap shells, such as CdS and ZnS, are deposited on the surface to construct core-shell QDs, their luminescence and photostability can be dramatically improved. This coating strategy has also been applied to enhance the fluorescence quantum yields of 1D semiconductor nanostructures, including NRs, NWs, arrows, and tetrapods, leading to unique optical and magnetic properties with diverse applications [94,95]. Additionally, metal ion doping represents another effective strategy for synthesizing brightly fluorescent QDs with low toxicity, such as Mn-doped ZnS and Cu-doped InZnS particles.

3.1.4. UCNPs

UCNPs, especially hexagonal $NaYF_4$ nanocrystals doped with trivalent lanthanide ions such as Er(III), Yb(III), or Tm(III), offer substantial advantages for fluorescence bioimaging, including minimal interference from autofluorescence, large anti-Stokes shifts, narrow emission spectra, excellent tissue penetration, and exceptional photostability [96]. UCNPs typically exhibit multiple emission colors, with the peak wavelengths varying according to the type of lanthanide dopant employed, which allows for improved microscopic resolution. The emission process of UCNPs differs from multi-photon processes because it entails the sequential absorption of two or more photons. Three types of upconversion mechanisms exist, i.e., excited state absorption (ESA), energy transfer upconversion (ETU), and photon avalanche. Upconversion nanocrystals generally comprise activators, sensitizers, and a host matrix, in which lanthanide ions (e.g., Er^{3+}, Tm^{3+}, and Ho^{3+}) are usually selected as activators and Yb^{3+} as the sensitizer. Rare-earth fluorides are commonly selected as host materials due to their comparable ionic sizes and chemical properties to lanthanide ions, as well as their low phonon energy and excellent stability [96]. The selective upregulation or downregulation of certain molecules, such as hydrogen sulfide (H_2S) and ROS, significantly affect important physiological processes. For example, metformin overdose can induce H_2S overexpression potentially leading to severe liver damage and toxicity. Consequently, a *Myrica rubra*-like nanoprobe with ratiometric fluorescence properties and orthogonal NIR-II emission was developed to accurately monitor the endogenous H_2S levels in real time and guide optimal oral medication dosing. This nanoprobe utilized a $NaYF_4$:Gd/Yb/Er@$NaYF_4$:Yb@SiO_2 core covered with Ag nanodots and was primarily taken up by the liver, featuring a sulfuration reaction-triggered conversion to a signal unit. The constructed sensing platform detected metformin-induced hepatotoxicity at a highly sensitive level of 0.7 nM and allowed for the ratiometric imaging of the varying degrees of hepatotoxicity *in situ* (Fig. 4D) [97]. The ROS, including O^{2-}, H_2O_2, ·OH, and ClO^- are critical in health and disease, particularly within cellular signaling systems, immune function, and organ injury. To address the drawbacks of inadequate biocompatibility, limited sensitivity, and susceptibility to photo-bleaching in previous ROS probes, Kuang and co-workers [98] fabricated a nanostructure featuring a UCNP core and chiral NiS_xNPs-functionalized zeolitic imidazolate framework-8 (ZIF-8) shell (UCNP@ZIF-NiS_x). This design achieved quantitative and selective monitoring of ROS *in vivo* through the degradation of NiS_x into UCNP@ZIF during the detection process. Particularly, $NaGdF_4$ is extensively employed as a positive contrast medium for MRI imaging. As a result, the optical properties of UCNPs can vary depending on the activators, sensitizers, host materials, as well as their crystal phases, particle sizes, and surface coatings [99]. Furthermore, the random migration of excitation energy from an atom to its neighboring atoms in a 1D atomic chain structure, 2D layer structure, and 3D structured crystal sublattice minimizes the

depletion of excitation energy and enhances the up-conversion at the sublattice level. This provides alternative prospects for engineering UCNPs for optical sensing and imaging applications [87]. However, the quantum yield of UCNPs is relatively lower than that of other fluorescent nanomaterials, and the synthesis of highly efficient UCNPs remains a great challenge.

3.2. 1D nanomaterials for multicolorimetric and SERS-based sensing

Unlike their 0D counterparts, 1D metal nanostructures, such as AuNRs and AgNWs, have notable optical properties for various applications. AuNRs are widely utilized in optical multicolorimetric sensing and imaging by simply altering the aspect ratio, which tunes their longitudinal LSPR peaks from visible to NIR wavelengths (650−1350 nm), where light penetrates tissues with the greatest efficiency [100]. Compared with AuNRs, AgNRs are also one of the most popular nanomaterials for LSPR shift-based sensing because of their narrower and intense spectra. Additionally, successful control of the aspect ratio of AgNRs causes a linear LSPR shift. Furthermore, controlling the exact shape, as well as formation of shells on the NRs and aggregation of 1D nanostructures, had been employed to adjust their optical characteristics [101]. To date, reports on the colloidal synthesis of 1D metal nanostructures have expanded from 2 (Au and Ag) to 23 different types. However, most of these methods still rely on capping agents for achieving anisotropic growth and precise aspect ratio control [64]. Anisotropic 1D metal nanostructures also serve as a key component in the construction of SERS-based sensors. However, the average EF for most plasmonic NP-based SERS sensors is less than 10^6 due to poor substrate reproducibility and misquoted SERS EF calculations. Depending on the aspect ratio control and analytes, the EF for Ag and AuNRs/AuNWs can be optimized to exceed 10^7 [102]. Choi and co-workers [103] developed a straightforward fabrication approach for a SERS sensor chip by attaching AuNPs onto vertically aligned zinc oxide NR (ZnO NR) arrays on cellulose paper. This setup achieved an enhanced Raman signal of 1.25×10^7. By utilizing a bioclassification method trained with machine learning and multivariate statistics, the proposed sensor chip could accurately predict and identify various types of prenatal diseases from minute quantities of genuine amniotic fluid with high sensitivity and specificity. Additionally, anisotropic nanomaterials and chiral assemblies possessing intense surface SERS signals are advantageous for identifying microRNAs (miRNAs) in a sequence-specific manner. Arrowhead-shaped AuNR dimers with both parallel and sequential arrangements were selectively modified with DNA and polyethylene glycol. The Raman signals of these dimers were significantly amplified. When the dimers recognized the target miRNAs, they disassembled evenly, resulting in a decrease in SERS signals, which enabled the efficient identification of target miRNAs and facilitated *in situ* Raman imaging (Fig. 4E) [104].

3.3. 2D and 3D nanomaterials for continuous molecular monitoring and/or targeted therapy

Ultrathin 2D metal nanomaterials typically present crystal structures identical to those of their corresponding bulk materials, with metal atoms closely arranged with neighboring atoms in face-centered cubic (FCC), hexagonal close-packed (HCP), or body-centered cubic (BCC) structures. Specifically, metals such as Au, Ag, Pt, Pd, Rh, and Ir typically crystallize in the standard FCC structure, whereas Ru and Os adopt an HCP phase [64]. Recently, reconfigurable arrangements of AuNPs, including linear assemblies (1D), monolayer films (MFGS), and superstructures with controlled particle spacing and arrangement, have provided new possibilities for optical sensing and catalytic applications [105,106]. Among these, 2D MFGS exhibit features such as accessible fabrication, strong stability, adjustable electromagnetic enhancement, unique optical absorption and electron transport abilities. The consistent arrangement of NPs in 2D MFGS not only enhances the stability and reliability of SERS detection by coupling hot spots but also enables multicolor displays in hybrid films [106]. Interfacial assembly is one of the primary methods for constructing optimized 2D MFGS due to its time-saving, simple fabrication procedure, and accurate regulation of the spatial distribution of AuNPs in the resulting films. Chen and co-workers [107] has promoted an interfacial chemical cross-linking strategy to assemble shrinkable AuNP MFGS and reoriented AuNRs on a Si substrate by increasing their interaction to achieve directional alignment. Moreover, recent studies have reported achievements in environmentally friendly and renewable 2D MFGS through the on-site reduction of AuNPs linked to polymers and the development of novel self-supporting 2D Janus AuNP films [108−110].

In contrast to microfluidic flexible electronics integrated biosensors and chromogenic agent-based wearable technology, optical wearable nanosensors based on 2D and 3D nanomaterials represent an emerging field that are still in their infancy. Undeniably, they offer unparalleled advantages for health monitoring because of their non-invasive nature, portability, and rapid responsiveness [111,112]. Various prototypes have been proposed for monitoring biomarkers on surface and in biofluids by using different smart nanomaterials. Zhou and co-workers [113] developed scalable and washing-reusable SERS membranes and textiles using a template-guided self-assembly method to incorporate AuNPs into highly hydrophobic microwell templates, which were then transferred via UV-curable resist-based micro/nanoimprinting. The proposed membranes exhibited promising potential for wearable biochemical sensing owing to their robust mechanical properties and the immobilization of UV-resistant AuNP aggregates. Notably, minimally invasive or noninvasive optical glucose sensors address the discomfort and procedural inconveniences associated with blood-based glucose self-testing. Tear fluid has been proposed as an alternative medium for reflecting glucose levels, providing a superior option for continuous *in vivo* and *in situ* testing. Chung and co-workers [114] designed a camera-oriented glucose optical monitoring system using cerium oxide NPs and glucose oxidase embedded in contact lenses. This system detects changes in tear glucose levels through color changes, eliminating the need for complex electronic components. Additionally, with the implementation of an image processing algorithm, the measurement accuracy is enhanced, even in the presence of image blurring, allowing for quantitative fully automatic efficacy to benefit patients with diabetes. Moreover, plasmonic nanostructures with SERS activity also facilitate *in situ* broad-spectrum molecular fingerprint identification at biointerfaces. Jung and co-workers [115] successfully demonstrated unconventional 3D plasmonic nanostructures exhibiting high SERS activity and consistency by employing nanotransfer printing. They further fabricated a SERS contact lens capable of measuring glucose levels in tears, achieving a linear range from 10^{-1} to 10^{-4} M (Fig. 5A) [115]. However, the optimization of the statistical quantification proved challenging owning to the substantial overlap between the primary SERS peaks of glucose and those of the monolayer. Consequently, for the practical implementation of nanomaterial-based SERS contact lenses, it is essential to validate the feasibility of retina-safe laser excitation and offer suitable guidelines. These aspects continue to be key objectives in advancing this technology. Moreover, for the real-time glucose monitoring, the inherently weak Raman signals and limited chemical affinity of glucose toward conventional SERS substrates, such as gold or silver, pose significant challenges.

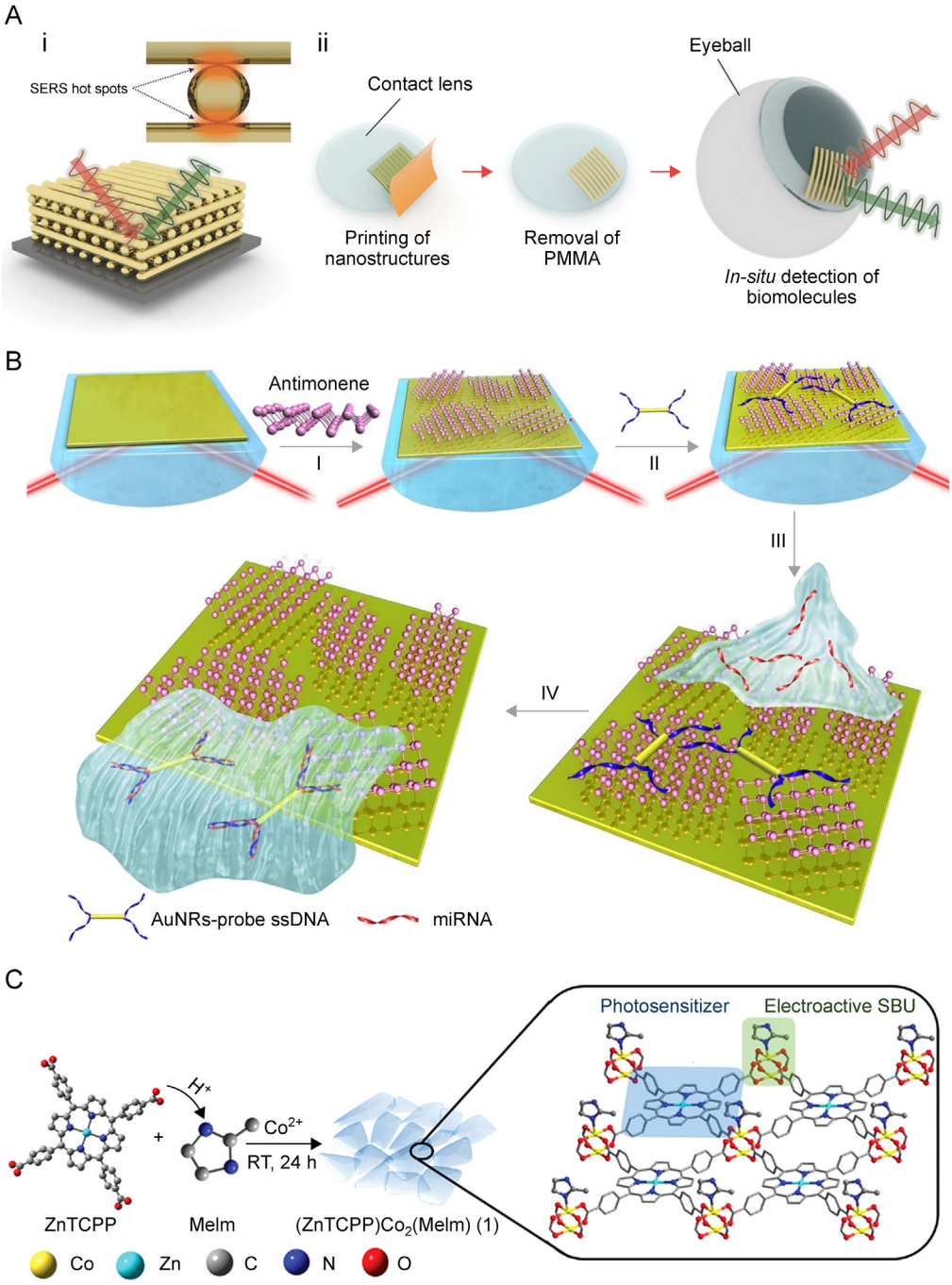

Fig. 5. Two-dimensional (2D) and 3D nanomaterials for continuous molecular monitoring and/or targeted therapy. (A) Schematic procedure for the fabrication of 3D cross-point nanostructures for surface enhancement Raman scattering (SERS) analysis (i) and schematic procedure for the fabrication of SERS contact lens via transfer printing for glucose detection (ii) [115]. (B) Schematic illustration of the strategy employed to detect microRNA (miRNA) hybridization events by assembling the antimonene nanosheets on the surface of Au film [125]. I–IV indicates the assembly of antimonene nanosheets on the Au film surface, the adsorption of gold nanorod (AuNR)-single stranded DNA (ssDNA) onto the antimonene nanosheets, the interaction of miRNA with AuNR-ssDNA on the antimonene surface, and the release of miRNA-bound AuNR-ssDNA from the antimonene nanosheets, respectively. (C) Design and construction of porphyrin-based heterobimetallic 2D metal-organic framework (MOF) [134]. PMMA: poly-methlymethacrylate; TCPP: tetrakis(4-carboxyphenyl)porphine; RT: room temperature; SBU: secondary building unit. Reproduced from Refs. [115,125,134] with permission.

Consequently, SERS-based glucose biosensors often employ linker molecules to enhance sensitivity and specificity. By reorganizing 3D AuNP clusters into a vertical-pillar configuration, the SERS emission shift of mercaptophenylboronic acid was correlated with glucose levels from 0.1 to 30 mM in aqueous humor and blood. Eye measurements using this platform aligned closely with those of commercial sensors, with a difference within 0.5 mM, highlighting its potential for extended continuous monitoring [116]. Recently, a wearable plasmonic sensor capable of recognizing a wide range of analytes was developed using a silver nanocube structure as the SERS-active component. This sensor was used for *in situ* monitoring of trace amounts of drugs in sweat, providing individual drug metabolic profiles and demonstrating its feasibility for universal and sensitive molecular tracking relevant to human health

assessment [117]. On the other hand, human skin serves as a sophisticated sensor that interacts with the surrounding environment and fosters numerous studies, including robotics, electronic-skin development, and human-computer interaction. A wearable electrochemiluminescence-based tactile sensors was designed with visual alarm features to prevent bodily harm from external stimuli by using carbon nanotubes (CNTs) embedded in polydimethylsiloxane as the electrode. Three specific luminophores producing red, green, and blue emissions were integrated into the electrochemiluminescence layer, enabling the continuous visualization of external stimuli by shape, size, and position [118]. Wang et al. [119] demonstrated a smart AuNCs-integrated antibacterial wound dressing capable of real-time monitoring of nanomedicine residues via *in situ* fluorescence, thereby facilitating timely dressing replacement. Taken together, nanomaterial-based optical biosensors for molecular drug or nano-drug monitoring and their beneficial aspects in biopharmaceutical applications especially for targeted therapy are summarized in Table 1 [42,62,70–74,76,79,85,97,119].

Nowadays, research has expanded from graphene to alternative ultrathin 2D nanomaterials, including TMDs, hexagonal boron nitride (h-BN), graphitic carbon nitride (g-C_3N_4), black phosphorus, and MXenes, among others [120]. These materials, with unique properties, such as substantial bandgaps, high conductivity, rapid electron transfer, and notable fluorescence, serve as transduction components and substrates for biosensing technologies. To enhance the sensitivity, surface chemistry modifications, such as defect engineering, doping, and creating heterostructures, are common. TMDs, in particular, are the most widely used in optical diagnostics, followed by MXenes, carbon nitrides, and BNs [63]. Some TMD QDs and g-C_3N_4 nanosheets exhibit strong fluorescence, enabling their use as fluorescent markers in protein assays and biomolecule identification [121]. Furthermore, 2D materials function as nanoquenchers, allowing distance-dependent fluorescence quenching tied to recognition events without the influence from donor emission spectra [63,122]. They are also employed in colorimetric systems because of their peroxidase-mimicking activity, with color responses observable by UV-vis spectrometry [123].

In contrast, nanozymes and 2D nanomaterials are prominent in tumor biomarker analyses. A hollow Janus hybrid nanozyme vector with dual-sided Ag—Au nanocages exhibits superior peroxidase-mimicking capabilities and precise targeting owing to its silver gate and DNAzyme nanobrushes. This “all-in-one” vector supports a stringent SERS liquid biopsy platform, achieving miRNA detection at 166 fM sensitivity [124]. Antimonene has demonstrated superior sensitivity compared with that of conventional 2D material graphene by exploring the chemical interactions between single-stranded DNA (ssDNA) and double-stranded DNA (dsDNA). Bao and co-workers [125] designed a SPR sensor for label-free molecular-level quantification and single nucleotide mutation identification, achieving unprecedented sensitivity in clinical nucleic acid detection. First, AuNRs were utilized to conjugate with ssDNA to enhance the SPR signal. Subsequently, the AuNR-ssDNA complex was adsorbed onto the antimonene nanosheets driven by the robust interaction between ssDNA and antimonene. Upon addition of complementary miRNA, the hybridized targets were readily desorbed from the antimonene surface, as dsDNA exhibited a weak binding affinity for antimonene. The miRNA concentration was quantified based on a negative shift in the SPR signal (Fig. 5B) [125]. Recently, composite systems of 2D materials have shown promising theranostic capabilities. For instance, Lin et al. [126] utilized soybean phospholipid-modified Ta_4C_3 nanosheets for dual-mode photoacoustic/computed tomography imaging and hyperthermia in tumors to demonstrate the photothermal efficiency of 4T1 breast cancer cells. Ji et al. [127] constructed a 2D MoS_2-glycoprobe (glycosheet) to control the ROS release from cells with asialoglycoprotein receptors.

Porous framework-based nanomaterials, which represent a class of typical 3D nanomaterials, are regarded as highly promising candidates for optical biosensing applications. In particular, MOFs and covalent organic frameworks (COFs) serve as two prominent representatives. The functionalization capabilities, uniform pore structures, and solvent stability of MOFs render them effective for selective optical sensing. Typically, MOFs comprise two primary elements: metal ions or clusters and organic linkers. These components are connected by precisely defined coordination bonds. An extensive variety of metal ions and metal clusters can be employed, while designable organic linkers offer further possibilities for tailoring the structure and physicochemical properties of MOFs. Owing to these versatile characteristics, a diverse array of MOFs have been successfully synthesized, including several well-known structures, such as MOF-5, HKUST-1, MIL-101, and UiO-66 [128]. Moreover, the isoreticular principle, which allows the modification of a structure's size and composition without altering its fundamental topology, is vital for designing and synthesizing MOFs with expanded pore sizes and increased pore volumes. This methodology has contributed to the development of an isoreticular series, such as isoreticular and zirconium-based MOFs, including UiO-66, UiO-67, and UiO-68 [128]. In the field of biosensing, specific pore sizes and functional ligands enable host-guest interactions at atomic level, and their varied optical and catalytic properties allow for the targeted detection of ions, gases, and biomolecules. Advanced optical techniques are now utilizing MOFs for complex biomarker diagnostics, including volatile organic compounds (VOCs). Qiao et al. [129] established a SERS-based VOC detection technique that enhanced Raman scattering for the early detection of lung malignancies. The ZIF-8 MOF shell layered on gold superparticles slowed the gaseous biomarker flow and optimized aldehyde detection for cancer diagnostics in mixed gases. Unlike inorganic platforms (e.g., QDs and noble metal NPs), MOFs are inherently degradable and biocompatible, offering non-toxic and highly stable sensing options [130]. Research on MOF-based chromism sensors is still in its early stages compared with that of the well-established noble metal-based colorimetric platforms. Typically, color changes in MOF chromic sensors arise through two main mechanisms: alterations in metal coordination geometry and shifts in charge transfer between the ground and excited electronic states [131]. When exposed to water vapor in air, the Cu^+-MOF assembled from CuI and 1-benzimidazolyl-3,5-*bis*(4-pyridyl)benzene acted as a sensitive colorimetric transducer that responded to air humidity by replacing the encapsulated organic molecules, producing a yellow-to-reddish-brown color shift corresponding to varying humidity levels [132]. In addition, reactive viologen groups incorporated into MOFs exhibit marked photochromism via charge transfer with electron-rich molecules (e.g., amines) upon light exposure, resulting in a dark-yellow to black color change [131]. In parallel, MOF-based luminescent systems have attracted considerable attention for biomedical and optical sensing applications. Numerous luminescent MOFs have been identified, with luminescence derived from organic ligands, emissive metal ions, guest ions, or fluorescent dyes encapsulated within the MOF pores, as well as from charge-transfer or catalytic activities. Ligands featuring aromatic or extended π-conjugation systems significantly contribute to MOF luminescence, and commonly used metal ions for functionalization include lanthanides, d10 transition metals, and silver clusters. In addition, encapsulating luminescent species such as QDs, metal complexes, organic dyes, and photosensitizers within MOF pores or through self-assembly further enhances MOF luminescence [133]. Recent advancements in MOF technology include the synthesis of a porphyrin-based heterobimetallic 2D

Table 1
Nanomaterial-based optical biosensors for molecular drug or nano-drug monitoring and their beneficial aspects in biopharmaceutical applications.

Type	Drug target	Sensing mechanism	Detection sensitivity	Nanomaterial type	Nanomaterial scale	Biological sample	Biopharmaceutical applications	Refs.
Molecular drug	Immunological or molecular targeted therapies	SERS	1 cell/mL	AuNPs	0D	10 patient blood samples	Monitoring phenotypic evolution of CTCs and providing vital tumour biology information for treatment management	[42]
	Lecithin	Electrochemiluminescence	0.05 mM	Single gold microbeads	0D	–	Evaluation excessive absorption or lack of lecithin	[62]
	Doxorubicin	LSPR and SERS	LSPR: 1 nM (in water) and 16 nM (in 10% fetal bovine serum/human serum); SERS: 100 pM (in water) and 1 nM (in 10% fetal bovine serum)	Gold nanoislands and Au/Al_2O_3 core/shell structures	0D	Fetal bovine serum/human serum samples	Continuous monitoring and adjustment of treatment dosage	[70]
	Crystal violet, mitoxantrone and methylene blue	SERS	10^{-13}, 8×10^{-10}, and 3×10^{-8} M, respectively	AgNPs assembled silver film and Au@AgNPs	3D and 0D	Mice	Pharmacokinetics investigation of two drugs (mitoxantrone and methylene blue) postintravenous injection in mice	[71]
	Mitoxantrone and methylene blue	SERS	2.9 and 193.8 nM, respectively	Core-satellite structured Au@AgNPs	0D	Dermal interstitial fluid of drug intravenously injected mice	Pharmacokinetics investigation of the two drugs in dermal interstitial fluid and blood	[72]
	Tobramycin	LSPR and SERS	LSPR: 20 μM; SERS: 4 μM	AuNPs	0D	Tobramycin spiked human serum	Ensurance of a safe and effective personalized dosage for infectious patients	[73]
	Heparin	Nanozyme catalysis	2×10^{-3} μg/mL	PtNCs	0D	Heparin spiked human serums	Providing guidance on medication dosage for clinical procedures	[79]
	Endogenous H_2S	NIR-II fluorescence	0.7 nM	$NaYF_4$:Gd/Yb/Er@$NaYF_4$:Yb@SiO_2@Ag_2S nanoprobe	0D	Metformin-induced hepatotoxicity mice model	*In situ* monitoring of metformin-induced hepatotoxicity	[97]
Nano-drug	Curcumin delivered photothermal nanomedicine	SERS	–	Waxberry-like AuNPs	0D	A549 cells and nude mice model	Investigating the *in vivo* dynamics of photothermal nanomedicines and delivered drug release	[74]
	AuNCs–Pt	Fluorescence	–	AuNCs–Pt	0D	Tumor cells	Visualization of tumor therapy	[76]
	Black-TiO_2 NPs	SERS	Single cancer cell	Black-TiO_2 NPs	0D	MCF-7 drug-resistant cancer cells	Visualization and photothermal therapy of drug-resistant cancer cells	[85]
	AuNCs	Fluorescence	–	AuNCs integrated dressing	0D	Sprague-Dawley rats with full-thickness infection skin wounds	Self-monitoring residue nanomedicine to indicate the appropriate time points for dressing replacement	[119]

–: no data. SERS: surface enhancement Raman scattering; AuNPs: gold nanoparticles; 0D: zero-dimensional; CTCs: circulating tumor cells; LSPR: localized surface plasmon resonance (SPR); NCs: nanoclusters; NIR: near-infrared.

MOF (Zn-porphyrin-based Co(II)-MOF) through the self-assembly of ZnTCPP and Co(II) salts in the presence of 2-methylimidazole (MeIm) at ambient temperature. The incorporation of paddlewhee [$Co_2(-CO_2)_4$] units facilitates electron transfer between the Co(II) ions and oxygen. This configuration enabled exceptional electrochemiluminescence performance, allowing the development of a non-amplified electrochemiluminescence biosensor based on this 2D MOF probe for the sensitive identification of the *RdRp* gene of SARS-CoV-2, demonstrating considerable potential for accurate viral detection (Fig. 5C) [134]. However, the specific geometric morphologies, limited functionalities, and unsatisfactory performances of pure MOFs restrict their broader applications. A large proportion of MOFs synthesized in deep eutectic solvents employ choline chloride/urea or its derivatives, whereas other combinations remain underexplored. Furthermore, the mechanisms governing surfactant interactions with metal ions and bridging ligands during the reaction process warrant further investigation. Innovations in 2D MOFs, such as conductive MOF nanosheets have also addressed the electrical limitations of MOF-based sensors. In contrast to MOFs, COFs are mainly constructed through covalent bonds with elements such as C, O, N, and B, and they show remarkable thermal and chemical stability. Guo et al. [135] fabricated COFs@MoS_2—Pd composites by incorporating MoS_2 nanosheets onto the surface of MoO_3@COFs microcables through a hydrothermal method, where the MoS_2 nanosheets acted as a support for the subsequent introduction of PdNPs. The incorporation of COF microtubes not only enhanced the electrical conductivity of the materials but also reduced the aggregation of MoS_2 nanosheets, thereby contributing to an enhancement in catalytic performance. The developed hybrids exhibited improved peroxidase-like activity and enabled selective colorimetric biosensing of uric acid. Moreover, COFs have also demonstrated considerable competitiveness in electrochemiluminescence-based biosensing. A COF exhibiting stable and intense electrochemiluminescent properties was prepared through the condensation reaction between perylene-3,4,9,10-tetracarboxylic dianhydride and melamine, functioned as a emitter. Upon the aptamer recognizing the pesticide residue of acetamiprid, the DNA trigger was released, subsequently activating the CRISPR/Cas12a system. This activation resulted in the cleavage of Fc-DNA and the initiation of the electrochemiluminescent signal. Moreover, the well-organized distribution of luminescent units within the COF structure, combined with the pore confinement effect, substantially improved the performance stability and sensitivity of the COF [136].

3.4. Nanocarbons for bioanalysis and bioimaging

Nanocarbons of various dimensions, such as 0D fullerenes and carbon/GQDs, 1D CNTs and graphene nanoribbons, 2D graphene and GOs, as well as 3D nanodiamonds, have gained substantial attention for their applications in refractive sensing and visualization because of their distinct characteristics of chemical inertness, size- and wavelength-dependent emission, resistance to photobleaching, broadband optical absorption, enzyme-like characteristics, ease of bioconjugation, simple and inexpensive synthesis without the need for heavy metal ions or organic solvents, low intrinsic toxicity, good cell permeability, and versatile surface functionalization. To date, in addition to the aforementioned nanomaterials, nanocarbon materials have also been extensively explored as alternative tools for developing next-generation optical biosensors designed for colorimetric/fluorescent detection, chemiluminescence, up-conversion PL, and fluorescence quenching, including FRET and CRET [137]. A comparison of detection performance based on diverse mechanisms and variously scaled nanomaterials for optical sensing is summarized in Table 2 [21–26,29–32,35,38–41,48–50,54,57,59,61,69,75,81,84,88–92,98,104,114–116,124,125,129,134,135,138–141]. Carbon QDs (CQDs), also known as carbon dots (CDs), are small clusters of carbon atoms with diameters smaller than 10 nm that possess semiconductor-like characteristics and are commonly used as substitutes for QDs in bioimaging. CQDs exhibit strong fluorescence without doping or labeling, with excitation and emission spectra typically extending from UV to red (650 nm) by varying the synthesis conditions (e.g., pH), sizes, morphologies, surface functionalities, and types or amounts of doping. Multi-photon excited CQDs facilitate multiplexing functions, and their fluorescence can be up-conversion or down-conversion [142]. As the basic building blocks of living organisms, cells convey tremendous amounts of genomic and transcriptomic information to sustain regular biochemical processes. Specifically, organelles, including the nucleus, mitochondria, and Golgi apparatus, are closely associated with tumorigenesis, cardiovascular, and neurodegenerative diseases. Thus, the *in situ* monitoring of organelle variations in cells is of great significance for early diagnosis and intervention. Shuang et al. [138] synthesized four types of CDs featuring distinct surface groups and varying degrees of lipophilicity for tunable organelle imaging through various uptake pathways, demonstrating their significant potential for specific organelle-targeting imaging in cell division and 3D reconstruction. GQDs, a type of CQD typically derived from graphene and/or GO, present graphene lattices that resemble the crystal structure of one or several graphene layers. GQDs typically have a diameters that range from 1 to 10 nm and are composed of fewer than 10 graphene layers. Compared with CQDs, GQDs typically exhibit stronger crystallinity and fewer defects owning to their higher proportion of crystalline sp^2 carbon. Both CQDs and GQDs generally possess numerous oxygen-based functional groups for surface modification, of which nitrogen doping is the most frequently used. Green luminescent GQDs have been successfully converted to blue luminescence via surface chemical modification with alkylamines. Similarly, GQDs modified with a combination of polyamidoamine and (3-aminopropyl)-triethoxysilane (APTES) showed an increased fluorescence intensity compared with that of CQDs modified with APTES or polyamidoamine individually, owning to the presence of multiple nitrogenous and oxygenated groups [142]. Functionalized spherical fullerenes (C_{60}), consisting of graphene in a spherical shape with pentagonal structures, serve as excellent nanomediators through functionalization or conjugation with amplification nanotags, such as AuNPs, to enhance the sensitivity of optical sensors. Increasing interest is focused on fluorescent fullerene NPs that exhibit tunable emission peaks based on their size and surface functional groups for multicolor optical sensing, both *in vitro* and *in vivo* [139]. Similar to CQDs and GQDs, 3D nanodiamonds can emit strong fluorescence owing to intrinsic nitrogen vacancy center defects, which serve as fluorescent emission centers. PL from these defect centers can be excited through both one-photon and two-photon stimulations [143]. The advantages of facile functionalization, nonphotobleaching, nonphotoblinking, and strong fluorescence intensity make nanodiamonds ideal for continuous cell tracking, although their rigid and costly preparation procedures limit large-scale use.

Since the unique fluorescence of individual single-walled CNTs (SWCNTs) was identified, substantial research has concentrated on exploiting the inherent optical properties of 1D nanocarbons, including SWCNTs and single-walled carbon nanohorns (SWCNHs) [87]. The composition of SWCNHs closely resembles that of SWCNTs, but with closed nanotubules forming into conical rather than tubular shapes. SWCNHs generally have diameters below 10 nm and lengths between 10 and 70 nm [137]. The indefinite photostability, single-molecule combination sensitivity, catalytic activity, and natural fluorescence in the NIR range provide

Table 2
A comparison of detection performance based on diverse mechanisms and variously scaled nanomaterials for optical sensing in biomedical applications.

Analyst type	Targets/analytes	Sensing mechanism	Detection sensitivity	Nanomaterial type	Nanomaterial scale	Biological samples	Refs.
Proteins	Interferon-gamma	LSPR/absorbance analysis	0.66 pg/mL	AuNRs	2D	–	[21]
	SCCA	LSPR peak shifts	0.85 ng/mL	AuNBP@Ag	2D	SCCA spiked human serums	[22]
	β-galactosidase (*E. coli*)	LSPR/colorimetric assay	128 pM (β-galactosidase); 1×10^4 CFU/mL (*E. coli* BL21)	Silver deposited AuNRs	2D	*E. coli*	[23]
	HCV antibody	Magnetic manipulation and LSPR detection	0.24 pg/mL	Core-shell-heterostructured magnetic-plasmonic nanoassemblies	0D	HCV-positive human serum samples	[25]
	SARS-CoV-2 IgG	Colorimetric and SERS dual-mode	10^{-7} mg/mL (colorimetric) and 0.22 pg/mL (SERS)	Ag^{MBA}@AuNPs	0D	107 clinical serum samples	[26]
	Heart-type fatty acid binding protein	Ratiometric fluorescence	0.21 ng/mL	AuNPs, CdSe/CdS/ZnS, and CdZnSe/CdS/ZnS QDs	0D	30 human serum samples	[29]
	IgE antibodies	Fluorescence	0.01–0.02 IU/mL	Tetrapod CdSe/CdS QDs-encoded microbeads	0D	10 cases of serum samples from healthy people and allergic patients	[30]
	Protein dimers on cell surface	Fluorescence turn-on	Single cell	DNA-templated AgNCs	0D	SKBR-3, MDA-MB-231, MCF-7, and MCF-10A cells	[31]
	Vasopressin, oxytocin, and 10 distinct amino acids	SERS	–	AuNSs trapped in a gold nanohole	0D	–	[38]
	Three globular proteins	SERS	–	AgNP-coated silica microbeads	0D	–	[39]
	Myeloperoxidase	BRET-FRET	–	Two tandem lipophilic dyes doped lipid nanobubble	–	An animal model of breast cancer	[59]
	Glutathione	Electrochemiluminescence	8.7×10^{-6} M	Au/AgNCs	0D	Glutathione spiked human serum samples	[61]
	Glutathione	Magnetic resonance/fluorescence	–	Core-shell metallofullerene	0D	Xenograft tumor mice models	[139]
Viruses	Influenza virus (HA1)	LSPR peak shifts and band-damping	1 fM	AuNRs and Pt@Ni nanorings	2D	–	[24]
DNAs/RNAs	MiR-141	SERS	0.03 fM	Silver stained AuNWs and Fe_3O_4@AuNPs	0D	Serum samples of 3 healthy volunteers and 3 prostate cancer patients	[35]
	Multiviral DNAs (*HBV*, *HPV*-16, and *HPV*-18)	SERS	1 aM	AuNPs and GO/triangle Au nanoflower array	0D and 2D	–	[69]
	SNPs in oncogenic Kirsten ras gene	Ratiometric fluorescence	4.6 nM	Hairpin DNA-templated AgNCs	0D	Single-base mismatched DNA target spiked cell lysate	[75]
	PCA3 sequence	MEF	1.42 pM	AuNRs and Ag_2S QDs	1D and 0D	MCF-7, Hela PC-3, and LNCap cells lysate	[90]
	MiR-21	SERS	0.023 and 0.011 amol/ng_{RNA} (side-by-side and end-to-end motifs, respectively)	Arrowhead AuNR dimers	2D	PCS-460-010, HeLa, and MCF-7 cells	[104]
	MiR-21	SERS	166 fM	Hollow Janus hybrid Ag–Au nanocages	1D and 3D	Human serum	[124]
	MiR-21 and MiR-155	SPR detection	10 aM	Antimonene nanosheets, Au film, AuNR-ssDNA	2D	–	[125]
	RdRp gene of SARS-CoV-2	Electrochemiluminescence	30 aM approximately	Zn-porphyrin-based Co(II)-MOF	2D	–	[134]
	SNPs in *TP53* gene	Nanozyme catalysis	0.11 nM	Hemin-CNT nanocomposites	1D	NCI–H661 and HUVEC cells	[140]
	HBV gene	Nanozyme catalysis	2 nM	Hemin-graphene hybrid nanosheets	2D	–	[141]
Cancer cells	CTCs	SERS	1 cell/mL	AuNPs, AuNRs, and AuNSs	0D and 1D	HepG2 and HeLa cells	[40]
	Heterogeneity of CTCs	SERS	Single cell	Silver shelled AuNPs	0D	32 SKBR3, 33 MCF7, 30 MDA-MB-231, and 31 Jurkat cells	[41]
	4T1 cancer cells	CRET	–	Hemoglobin and luminol combined MOF	3D	4T1 tumor-bearing mice	[54]
	Deep tumor *in vivo* imaging	BRET	–	NanoLuc luciferase conjugated Ag_2S QDs	0D	Murine 4T1 breast cancer tumor model	[57]
	CTCs	SERS	1 cell/mL	Octahedral Ag_2O NPs	0D	Human blood	[84]
	CTCs	Fluorescence	Single cell		0D		[88]

(*continued on next page*)

Table 2 (*continued*)

Analyst type	Targets/analytes	Sensing mechanism	Detection sensitivity	Nanomaterial type	Nanomaterial scale	Biological samples	Refs.
				DNA-templated magnetic NP-QD-aptamer copolymers		Human leukemia CCRF-CEM cells; blood samples	
	A549 lung cancer cells (mucin 1)	Fluorescence	3 cells/mL (A549 cells) and 0.15 fg/mL (mucin 1)	CdTe QDs	0D	51 clinical blood samples of lung cancer patients	[89]
	HeLa cells (HSP90, Ki-67, lamin A, calnexin, and β-tubulin)	Fluorescence	Single cell	QDs	0D	HeLa cells	[92]
	Organelles	Fluorescence	–	CDs	0D	LoVo, bEnd.3, HC11, MCF-7, HepG2 cells; zebrafish	[138]
Small molecules	Glucose and cholesterol	Colorimetric and fluorescence	53.39 μM (colorimetric) and 41.90 μM (fluorescent)	Biodot@AgNPs nanohybrid	0D	Synthetic urine and human plasma	[32]
	Glucose	Nanozyme catalysis	8.5 mM	AuNPs/Cu-TCPP(M) hybrid nanosheets (M = Fe, Co)	0D and 2D	–	[48]
	Glucose and cholesterol	Nanozyme catalysis	–	Cyclodextrin@AuNPs and nanosuperstructures	0D, 1D, or 2D	Human serum samples	[49]
	Glucose	Nanozyme catalysis	1×10^{-6} M	MnO_2 nanoflakes	2D	Human blood serum samples	[50]
	Glucose and glutathione	Nanozyme catalysis	0.16 μM (glucose) and 120 nM (glutathione)	Integration $CoFe_2O_4$ with porous carbon	0D	Goat serums	[81]
	Cysteine	Fluorescence	50 nM	N-GQDs@V_2O_5 nanosheets	2D	Human serum samples	[91]
	ROS	Fluorescence	0.037 μM	UCNP@ZIF-NiSx	3D	Normal primary uterine fibroblast cells and HeLa-tumor bearing-mouse	[98]
	Tear glucose	Colorimetric	0.1 mM	Cerium oxide NPs	0D	Diabetic transgenic mice and human tear (4 diabetic patients and 4 healthy subjects)	[114]
	Tear glucose	SERS	0.1 mM	Multistacked 3D crossed-AuNWs	3D	An artificial glass eye	[115]
	Continuous glucose sensing	SERS	0.1 mM	Stacked AuNP clusters	3D	6 *ex vivo* rabbit eyes (rabbit anterior chambers)	[116]
	VOCs (gaseous aldehydes)	SERS	10 ppb	GSPs@ZIF-8	3D	–	[129]
	Uric acid	Nanozyme catalysis	–	COFs@MoS_2–Pd	3D	–	[135]

–: no data. SCCA: squamous cell carcinoma-antigen; LSPR: localized surface plasmon resonance (SPR); AuNRs: gold nanorods; 2D: two-dimensional; AuNBP@Ag: Ag-shelled Au@Ag NRs; *E. coli*: *Escherichia coli*; HCV: hepatitis C virus; SARS-CoV-2: severe acute respiratory syndrome coronavirus 2; SERS: surface enhancement Raman scattering; MBA: 4-mercaptobenzoic acid; NP: nanoparticle; QDs: quantum dots; NCs: nanoclusters; AuNSs: gold nanostars; BRET: bioluminescence resonance energy; FRET: Förster resonance energy transfer; AuNWs: gold nanowires; GO: graphene oxide; SNPs: single nucleotide polymorphisms; MEF: metal-enhanced fluorescence; ng_{RNA}: each nanogram (ng) of RNA ssDNA: single-stranded DNA; MOF: metal-organic framework; CNT: carbon nanotube; HUVEC: human umbilical vein endothelial cells; CTCs: circulating tumor cells; CRET: chemiluminescence resonance energy transfer; CDs: carbon dots; TCPP: tetrakis(4-carboxyphenyl)porphine; N-GQDs: nitrogen-doped graphene QDs; ROS: reactive oxygen species; UCNP@ZIF-NiSx: an upconversion NP (UCNP) core and a zeolitic imidazolate framework-8 (ZIF-8) shell encapsulated with chiral NiSxNPs; VOC: volatile organic compound; GSPs: gold superparticles; COFs: covalent organic frameworks.

substantial potential for detection systems in various applications. However, a major challenge in developing CNT-based materials is mitigating their tendency to self-associate in water, forming thick, insoluble, and potentially harmful aggregates. Surface functionalization strategies, including both covalent and non-covalent modifications of the sidewalls, have been adopted to improve dispersibility and biocompatibility. Carboxylated SWCNTs can be covalently fabricated using AuNPs, QDs, and superparamagnetic iron oxide NPs for multifunctional imaging. In SWCNT immunoassays, avidin and biotin functional groups are also widely employed as linkers for additional labels [144]. In contrast to covalent methods, non-covalent wrappings or decorations avoid modifying the extended π-conjugated system and optical properties of SWCNTs while stabilizing them in water, imparting additional attributes, such as molecular recognition. Biopolymers, including DNA, RNA, peptides, and proteins, have considerable advantages for improving SWCNT-based optical sensors for label-free target detection. Moreover, SWCNTs exhibit peroxidase-like properties, which are influenced by pH, temperature, and H_2O_2 concentration, resembling HRP activity. These properties have been utilized to develop optical biosensing platforms [140,145]. In contrast, SWCNHs, arranged in round clusters resembling dahlia flowers owning to van der Waals forces between exposed ends, ranged in size from 40 to 200 nm. This structure provides a higher surface-to-volume ratio than that of SWCNTs, enabling more efficient functionalization with biomolecules or NPs for fluorescence labeling [146].

Graphene nanosheets, 2D atomic-thin layer materials with zero bandgap (~0.34 nm) as the fundamental unit due to their sp^2 hybridization, have numerous functional characteristics, including high conductivity, intrinsic catalytic activity, low cytotoxicity, and an exceptionally large surface area (up to 2630 m^2/g) with each carbon atom exposed. Since graphene was isolated from bulk graphite, it has been widely studied for applications in highly sensitive fluorescence-quenching biosensors, Raman imaging, and nanozyme-based bioanalysis across multiple fields [147]. The GO

nanosheets have been extensively used as highly responsive signal indicators for detecting biomolecules and effective nanocarriers due to uniform size, excellent solubility, biocompatibility, and inherent NIR PL, making them suitable for cellular imaging with minimal background interference [148]. Moreover, numerous carbon-based composites, such as hemin-graphene and PtAuNP-GO, have functioned as peroxidase mimics for H_2O_2, oxidase substrates, ions, nucleic acid, and protein detection [141,147]. Guo et al. [141] synthesized hemin-graphene hybrid nanosheets that exhibit intrinsic peroxidase-like activity. By exploiting the distinct affinities of ssDNA and dsDNA to these nanosheets, a label-free colorimetric detection method for *HBV* DNA was established, achieving a LOD as low as 2 nM. Moreover, this sensor demonstrated sufficient selectivity to effectively distinguish single-base mismatches.

4. Conclusion

Advancements in functionalized low-dimensional nanomaterials have accelerated the development of optical biosensors, supporting a range of biomedical research and biopharmaceutical applications, including IVDs, POC tools, therapeutic drug monitoring, bioimaging, targeted therapy, and wearable and implantable systems for continuous drug monitoring. This review systematically summarizes the underlying design principles for assembling optical sensors and highlights the specific advantages and properties of smart nanomaterials for each type of biosensor. Notably, nanomaterial-functionalized LSPR-based POC nanosystems offer a compelling approach by converting target recognition into absorption band shifts and color variations readily observable by the unaided eye. Further advances in multicolorimetric strategies based on etching and growth mechanisms have enabled the semi-quantification of targets, often using noble metal nanomaterials, such as 1D anisotropic AuNRs and Au@Ag nanocomposites. As metal nanomaterials shrink below 2 nm, their unique photoluminescent properties emerge, with the disappearance of the LSPR phenomenon.

Current ratiometric fluorescence platforms have achieved high visual resolution using novel nanomaterials, such as DNA-templated AgNCs, CdSe, and CdTe-based QDs, NIR Ag_2S QDs, CDs/GQDs, lanthanide-doped UCNPs, TMD QDs, and g-C_3N_4 nanosheets. Dual-mode sensing platforms combining colorimetric, fluorescence, or SERS readouts are particularly competitive in IVD and POC applications. SERS spectroscopy is especially powerful, using large-volume “hot spots” of nanomaterials to amplify target signals, facilitating single-molecule analysis and CTCs detection. However, the high cost of noble metals limits the large-scale preparation of these materials, prompting interest in low-cost oxides with considerable stability in nanozymes and SERS platforms for the detection of biomolecules, such as glucose, xanthine, and cholesterol. Meanwhile, chemiluminescence and bioluminescence-based sensors show promising capabilities for probing biological specimens and detecting cell damage or disease through *in vivo* imaging. By eliminating external light excitation with CRET and BRET, these sensors can overcome challenges such as fluorescence quenching and poor tissue penetration. Electrochemiluminescence systems generate luminescent signals via nanomaterial-based electrochemiluminescence probes for biosensing and high-throughput drug monitoring, with further development of optical wearable nanosensors relying on 1D CNT-embedded electrodes. Additionally, 2D MFGS and uniform 3D cross-point plasmonic nanostructures have potential for use in SERS-based wearable biochemical sensors and theranostic applications in continuous drug monitoring and targeted therapy. Altogether, nanomaterial-functionalized optical biosensors are undergoing rapid evolution and extensive growth.

However, several challenges remain unaddressed. Current deficiencies include the need for reliable and accurate POC tools for rapid viral detection, miniaturized sensors for real-time at-home monitoring (such as wearable or implantable nanosensors), and simplified read-out devices that are easily observable without aid. Although the integration of nanomaterials enhances the feasibility and rapidness of their target detection and monitoring, the sensitivity of nanomaterials to varying sensing conditions and tendency to form non-reversible aggregates must be addressed to improve their functionalization and storage stability. Additionally, innovative preparation and fabrication methods for cost-effective and low-toxicity nanostructures that leverage machine learning remain urgent priorities because the controlled preparation process is still poorly understood, with most methods have been developed through trial and error. For *in vivo* monitoring and integrated theranostic systems, the biological toxicity and metabolic characteristics of nanomaterials also require comprehensive investigation. Future directions in nanomaterial-based optical biosensors should focus on bridging the gap between academic research and commercial applications, addressing biomedical and pharmaceutical complexities by integrating advances in spectroscopic instrumentation with recent developments in nanofabrication technologies.

CRediT authorship contribution statement

Mengjia Xu: Writing – review & editing, Writing – original draft, Visualization. **Lutfun Nahar:** Writing – review & editing, Validation, Supervision. **Kenneth J. Ritchie:** Supervision, Investigation. **Chenxu Wang:** Visualization. **Li Cheng:** Resources, Investigation. **Zimiao Wu:** Resources, Investigation. **Satyajit D. Sarker:** Writing – review & editing, Resources, Investigation, Conceptualization. **Mingquan Guo:** Writing – review & editing, Validation, Conceptualization, Funding acquisition, Resources.

Declaration of competing interest

The authors declare that there are no conflicts of interest.

Acknowledgments

This work was supported by the National Natural Science Foundation of China (Grant No.: 32101921), Ningbo Natural Science Foundation, China (Project Nos.: 2023J001 and 2024J255), the Key Science and Technology Project of Ministry of Emergency Management of the People’s Republic of China (Grant No.: 2024EMST141408), Ningbo Yongjiang Talent Introduction Program, China (Program No.: 2022A-078-G), the Key Project of Ningbo Public Welfare Science and Technology, China (Project No.: 2024S037), Ningbo Leading Medical & Health Discipline, China (Project No.: 2022-X22), Project of Cixi Leading Medical & Health Discipline, China (Project No.: 2023-ZD07), The European Regional Development Fund - Project ENOCH (Project No.: CZ.02.1.01/0.0/0.0/16_019/0000868), the Czech Agency Grants, Czech Republic (Project Nos.: 23-05474S and 23-05389S), and the Chinese Academy of Sciences President’s International Fellowship Initiative, China (Project No.: 2025PVA0074).

Appendix A. Supplementary data

Supplementary data to this article can be found online at https://doi.org/10.1016/j.jpha.2025.101349.

References

[1] F. Scheller, F. Schubert, D. Pfeiffer, et al., Research and development of biosensors. a review, Analyst 114 (1989) 653–662.

[2] D.R. Thévenot, K. Toth, R.A. Durst, et al., Electrochemical biosensors: recommended definitions and classification, Biosens. Bioelectron. 16 (2001) 121–131.
[3] F.S. Ligler, Perspective on optical biosensors and integrated sensor systems, Anal. Chem. 81 (2009) 519–526.
[4] Y. Yang, W. Gao, Wearable and flexible electronics for continuous molecular monitoring, Chem. Soc. Rev. 48 (2019) 1465–1491.
[5] J. Kim, Y. Lee, M. Kang, et al., 2D materials for skin-mountable electronic devices, Adv. Mater. 33 (2021), 2005858.
[6] F.S. Ligler, J.J. Gooding, Lighting up biosensors: now and the decade to come, Anal. Chem. 91 (2019) 8732–8738.
[7] J.R. Askim, M. Mahmoudi, K.S. Suslick, Optical sensor arrays for chemical sensing: the optoelectronic nose, Chem. Soc. Rev. 42 (2013) 8649–8682.
[8] S. Shrivastava, T.Q. Trung, N.E. Lee, Recent progress, challenges, and prospects of fully integrated mobile and wearable point-of-care testing systems for self-testing, Chem. Soc. Rev. 49 (2020) 1812–1866.
[9] J. Kirsch, C. Siltanen, Q. Zhou, et al., Biosensor technology: recent advances in threat agent detection and medicine, Chem. Soc. Rev. 42 (2013) 8733–8768.
[10] M. Tian, Z. Yuan, Y. Liu, et al., Recent advances of plasmonic nanoparticle-based optical analysis in homogeneous solution and at the single-nanoparticle level, Analyst 145 (2020) 4737–4752.
[11] C. Jin, Z. Wu, J.H. Molinski, et al., Plasmonic nanosensors for point-of-care biomarker detection, Mater. Today Bio 14 (2022), 100263.
[12] C. Tan, X. Cao, X. Wu, et al., Recent advances in ultrathin two-dimensional nanomaterials, Chem. Rev. 117 (2017) 6225–6331.
[13] F. Wang, A. Dong, W.E. Buhro, Solution-liquid-solid synthesis, properties, and applications of one-dimensional colloidal semiconductor nanorods and nanowires, Chem. Rev. 116 (2016) 10888–10933.
[14] H. Yoo, H. Jo, S.S. Oh, Detection and beyond: challenges and advances in aptamer-based biosensors, Mater. Adv. 1 (2020) 2663–2687.
[15] Q. Xue, Z. Li, Q. Wang, et al., Nanostrip flexible microwave enzymatic biosensor for noninvasive epidermal glucose sensing, Nanoscale Horiz 5 (2020) 934–943.
[16] M. Qi, D. Lv, Y. Zhang, et al., Development of a surface plasmon resonance biosensor for accurate and sensitive quantitation of small molecules in blood samples, J. Pharm. Anal. 12 (2022) 929–936.
[17] W. Wei, K. Chen, G. Ge, Strongly coupled nanorod vertical arrays for plasmonic sensing, Adv. Mater. 25 (2013) 3863–3868.
[18] S. Zeng, D. Baillargeat, H.P. Ho, et al., Nanomaterials enhanced surface plasmon resonance for biological and chemical sensing applications, Chem. Soc. Rev. 43 (2014) 3426–3452.
[19] X. Ma, S. He, B. Qiu, et al., Noble metal nanoparticle-based multicolor immunoassays: an approach toward visual quantification of the analytes with the naked eye, ACS Sens. 4 (2019) 782–791.
[20] H. Rao, X. Xue, H. Wang, et al., Gold nanorod etching-based multicolorimetric sensors: strategies and applications, J. Mater. Chem. C 7 (2019) 4610–4621.
[21] B. Liu, Y. Cheng, X. Pan, et al., Multicolor-assay-on-a-chip processed by robotic operation (MACpro) with improved diagnostic accuracy for field-deployable detection, Anal. Chem. 96 (2024) 6634–6642.
[22] Y. Lin, S. Xu, J. Yang, et al., Interesting optical variations of the etching of Au Nanobipyramid@Ag Nanorods and its application as a colorful chromogenic substrate for immunoassays, Sensor. Actuator. B Chem. 267 (2018) 502–509.
[23] J. Chen, A.A. Jackson, V.M. Rotello, et al., Colorimetric detection of *Escherichia coli* based on the enzyme-induced metallization of gold nanorods, Small 12 (2016) 2469–2475.
[24] H. Hilal, S. Lee, I. Jung, et al., Scattering fourier transform biosensor: binary mixture consisting of magnetic Ni nanorings and plasmonic Au nanorods, Anal. Chem. 92 (2020) 10099–10107.
[25] L. Hao, Y. Leng, L. Zeng, et al., Core-shell-heterostructured magnetic-plasmonic nanoassemblies with highly retained magnetic-plasmonic activities for ultrasensitive bioanalysis in complex matrix, Adv. Sci. 7 (2020), 1902433.
[26] P. Liang, Q. Guo, T. Zhao, et al., Ag nanoparticles with ultrathin Au shell-based lateral flow immunoassay for colorimetric and SERS dual-mode detection of SARS-CoV-2 IgG, Anal. Chem. 94 (2022) 8466–8473.
[27] Z. Li, Q. Sun, Y. Zhu, et al., Ultra-small fluorescent inorganic nanoparticles for bioimaging, J. Mater. Chem. B 2 (2014) 2793–2818.
[28] X. Huang, J. Song, B.C. Yung, et al., Ratiometric optical nanoprobes enable accurate molecular detection and imaging, Chem. Soc. Rev. 47 (2018) 2873–2920.
[29] J. Wang, C. Jiang, J. Jin, et al., Ratiometric fluorescent lateral flow immunoassay for point-of-care testing of acute myocardial infarction, Angew. Chem. Int. Ed. 60 (2021) 13042–13049.
[30] W. Wu, X. Yu, M. Gao, et al., Precisely encoded barcodes using tetrapod CdSe/CdS quantum dots with a large stokes shift for multiplexed detection, Adv. Funct. Mater. 30 (2020), 1906707.
[31] L. Xu, Z. Zhou, X. Gou, et al., Light up multiple protein dimers on cell surface based on proximity-induced fluorescence activation of DNA-templated sliver nanoclusters, Biosens. Bioelectron. 179 (2021), 113064.
[32] H.V. Xu, Y. Zhao, Y.N. Tan, Nanodot-directed formation of plasmonic-fluorescent nanohybrids toward dual optical detection of glucose and cholesterol via hydrogen peroxide sensing, ACS Appl. Mater. Interfaces 11 (2019) 27233–27242.
[33] X. Wang, S. Huang, S. Hu, et al., Fundamental understanding and applications of plasmon-enhanced Raman spectroscopy, Nat. Rev. Phys. 2 (2020) 253–271.
[34] S. Schlücker, Surface-enhanced Raman spectroscopy: concepts and chemical applications, Angew. Chem., Int. Ed. 53 (2014) 4756–4795.
[35] H. Shao, H. Lin, Z. Guo, et al., A multiple signal amplification sandwich-type SERS biosensor for femtomolar detection of miRNA, Biosens. Bioelectron. 143 (2019), 111616.
[36] M.A. Tahir, N.E. Dina, H. Cheng, et al., Surface-enhanced Raman spectroscopy for bioanalysis and diagnosis, Nanoscale 13 (2021) 11593–11634.
[37] E. Garcia-Rico, R.A. Alvarez-Puebla, L. Guerrini, Direct surface-enhanced Raman scattering (SERS) spectroscopy of nucleic acids: from fundamental studies to real-life applications, Chem. Soc. Rev. 47 (2018) 4909–4923.
[38] J.A. Huang, M.Z. Mousavi, G. Giovannini, et al., Multiplexed discrimination of single amino acid residues in polypeptides in a single SERS hot spot, Angew. Chem., Int. Ed. 59 (2020) 11423–11431.
[39] X. Dai, W. Fu, H. Chi, et al., Optical tweezers-controlled hotspot for sensitive and reproducible surface-enhanced Raman spectroscopy characterization of native protein structures, Nat. Commun. 12 (2021), 1292.
[40] X. Wu, Y. Xia, Y. Huang, et al., Improved SERS-active nanoparticles with various shapes for CTC detection without enrichment process with super-sensitivity and high specificity, ACS Appl. Mater. Interfaces 8 (2016) 19928–19938.
[41] Y. Zhang, Z. Wang, L. Wu, et al., Combining multiplex SERS nanovectors and multivariate analysis for *in situ* profiling of circulating tumor cell phenotype using a microfluidic chip, Small 14 (2018), e1704433.
[42] S.C. Tsao, J. Wang, Y. Wang, et al., Characterising the phenotypic evolution of circulating tumour cells during treatment, Nat. Commun. 9 (2018), 1482.
[43] J. Wu, X. Wang, Q. Wang, et al., Nanomaterials with enzyme-like characteristics (nanozymes): next-generation artificial enzymes (II), Chem. Soc. Rev. 48 (2019) 1004–1076.
[44] X. Wu, T. Chen, J. Wang, et al., Few-layered $MoSe_2$ nanosheets as an efficient peroxidase nanozyme for highly sensitive colorimetric detection of H_2O_2 and xanthine, J. Mater. Chem. B 6 (2018) 105–111.
[45] W. Zhao, G. Zhang, Y. Du, et al., Sensitive colorimetric glucose sensor by iron-based nanozymes with controllable Fe valence, J. Mater. Chem. B 9 (2021) 4726–4734.
[46] D. Mao, W. Li, F. Zhang, et al., Nanocomposite of peroxidase-like cucurbit[6]uril with enzyme-encapsulated ZIF-8 and application for colorimetric biosensing, ACS Appl. Mater. Interfaces 13 (2021) 39719–39729.
[47] J. Xiao, Y. Liu, L. Su, et al., Microfluidic chip-based wearable colorimetric sensor for simple and facile detection of sweat glucose, Anal. Chem. 91 (2019) 14803–14807.
[48] Y. Huang, M. Zhao, S. Han, et al., Growth of Au nanoparticles on 2D metalloporphyrinic metal-organic framework nanosheets used as biomimetic catalysts for cascade reactions, Adv. Mater. 29 (2017), 1700102.
[49] Y. Zhao, Y. Huang, H. Zhu, et al., Three-in-one: sensing, self-assembly, and cascade catalysis of cyclodextrin modified gold nanoparticles, J. Am. Chem. Soc. 138 (2016) 16645–16654.
[50] L. Han, H. Zhang, D. Chen, et al., Protein-directed metal oxide nanoflakes with tandem enzyme-like characteristics: Colorimetric glucose sensing based on one-pot enzyme-free cascade catalysis, Adv. Funct. Mater. 28 (2018), 1800018.
[51] M. Yang, J. Huang, J. Fan, et al., Chemiluminescence for bioimaging and therapeutics: recent advances and challenges, Chem. Soc. Rev. 49 (2020) 6800–6815.
[52] Y. Sun, Y. Gao, C. Tang, et al., Multiple rapid-responsive probes for hypochlorite detection based on dioxetane luminophore derivatives, J. Pharm. Anal. 12 (2022) 446–452.
[53] Y. Zhong, J. Li, A. Lambert, et al., Expanding the scope of chemiluminescence in bioanalysis with functional nanomaterials, J. Mater. Chem. B 7 (2019) 7257–7266.
[54] L. Hu, C. Xiong, J. Zou, et al., Engineered MOF-enzyme nanocomposites for tumor microenvironment-activated photodynamic therapy with self-luminescence and oxygen self-supply, ACS Appl. Mater. Interfaces 15 (2023) 25369–25381.
[55] Y. Jiang, K. Pu, Molecular probes for autofluorescence-free optical imaging, Chem. Rev. 121 (2021) 13086–13131.
[56] A.J. Syed, J.C. Anderson, Applications of bioluminescence in biotechnology and beyond, Chem. Soc. Rev. 50 (2021) 5668–5705.
[57] M.J. Afshari, C. Li, J. Zeng, et al., Self-illuminating NIR-II bioluminescence imaging probe based on silver sulfide quantum dots, ACS Nano 16 (2022) 16824–16832.
[58] R. Alam, L.M. Karam, T.L. Doane, et al., Probing bioluminescence resonance energy transfer in quantum rod-luciferase nanoconjugates, ACS Nano 10 (2016) 1969–1977.
[59] R. Liu, J. Tang, Y. Xu, et al., Bioluminescence imaging of inflammation *in vivo* based on bioluminescence and fluorescence resonance energy transfer using nanobubble ultrasound contrast agent, ACS Nano 13 (2019) 5124–5132.
[60] Y. Chen, Y. Cao, C. Ma, et al., Carbon-based dots for electrochemiluminescence sensing, Mater. Chem. Front. 4 (2020) 369–385.
[61] C. Han, W. Guo, Fluorescent noble metal nanoclusters loaded protein hydrogel exhibiting anti-biofouling and self-healing properties for electrochemiluminescence biosensing applications, Small 16 (2020), e2002621.
[62] G. Liu, P. Wang, H. Gao, Visualization analysis of lecithin in drugs based on electrochemiluminescent single gold microbeads, J. Pharm. Anal. 11 (2021) 515–522.

[63] N. Rohaizad, C.C. Mayorga-Martinez, M. Fojtů, et al., Two-dimensional materials in biomedical, biosensing and sensing applications, Chem. Soc. Rev. 50 (2021) 619–657.
[64] D. Huo, M.J. Kim, Z. Lyu, et al., One-dimensional metal nanostructures: from colloidal syntheses to applications, Chem. Rev. 119 (2019) 8972–9073.
[65] F. He, H. Wang, P. Du, et al., Personal glucose meters coupled with signal amplification technologies for quantitative detection of non-glucose targets: recent progress and challenges in food safety hazards analysis, J. Pharm. Anal. 13 (2023) 223–238.
[66] X. Zhu, Y. Zhang, M. Liu, et al., 2D titanium carbide MXenes as emerging optical biosensing platforms, Biosens. Bioelectron. 171 (2021), 112730.
[67] Y. Liu, P. Li, R. Cui, et al., Metal-organic frameworks (MOFs) and covalent organic frameworks (COFs)-based prototyping of integrated sensing devices for robust analysis, TrAC, Trends Anal. Chem. 174 (2024), 117678.
[68] J. Sun, Y. Xianyu, X. Jiang, Point-of-care biochemical assays using gold nanoparticle-implemented microfluidics, Chem. Soc. Rev. 43 (2014) 6239–6253.
[69] J.H. Choi, M. Shin, L. Yang, et al., Clustered regularly interspaced short palindromic repeats-mediated amplification-free detection of viral DNAs using surface-enhanced Raman spectroscopy-active nanoarray, ACS Nano 15 (2021) 13475–13485.
[70] A. Quarta, S. Bettini, M. Cuscunà, et al., Tailoring gold nanoisland-based biosensors for ultrasensitive detection of doxorubicin in biological fluids, ACS Appl. Nano Mater. 7 (2024) 18724–18736.
[71] B. Lv, Y. Wang, R. Mei, et al., Enhanced superhydrophobic substrate-based 3D SERS platform for a portable Raman spectrometer-assisted drug detection in plasma, ACS Appl. Nano Mater. 7 (2024) 14665–14672.
[72] Y. Li, Y. Wang, R. Mei, et al., Hydrogel-coated SERS microneedles for drug monitoring in dermal interstitial fluid, ACS Sens. 9 (2024) 2567–2574.
[73] K.S. McKeating, M.P. Couture, M. Dinel, et al., High throughput LSPR and SERS analysis of aminoglycoside antibiotics, Analyst 141 (2016) 5120–5126.
[74] R. Mei, Y. Wang, X. Zhao, et al., Near-infrared light-responsive SERS tags enable positioning and monitoring of the drug release of photothermal nanomedicines *in vivo*, Anal. Chem. 93 (2021) 16590–16597.
[75] M. Xu, X. Wang, J. Tian, et al., A clamp-improved universal amplified system for ratiometric fluorescent detection of single-nucleotide polymorphisms coupled with a novel dual-emissive silver nanocluster, Sensor. Actuator. B Chem. 367 (2022), 132151.
[76] Y. Yang, Y. Yu, H. Chen, et al., Illuminating platinum transportation while maximizing therapeutic efficacy by gold nanoclusters *via* simultaneous near-infrared-I/II imaging and glutathione scavenging, ACS Nano 14 (2020) 13536–13547.
[77] B. Casteleiro, J.M.G. Martinho, J.P.S. Farinha, Encapsulation of gold nanoclusters: stabilization and more, Nanoscale 13 (2021) 17199–17217.
[78] M. Li, Y. Xie, J. Zhang, et al., Self-assembled integrated nanozyme cascade biosensor with dual catalytic activity for portable urease analysis, Anal. Chem. 96 (2024) 1284–1292.
[79] X. Li, Q. Huang, W. Li, et al., *N*-acety-L-cysteine-stabilized Pt nanozyme for colorimetric assay of heparin, J. Anal. Test. 3 (2019) 277–285.
[80] L. Chen, Z. Liu, Z. Guo, et al., Regulation of intrinsic physicochemical properties of metal oxide nanomaterials for energy conversion and environmental detection applications, J. Mater. Chem. A 8 (2020) 17326–17359.
[81] J. Luo, R. Liu, S. Zhao, et al., Bimetallic Fe-Co nanoalloy confined in porous carbon skeleton with enhanced peroxidase mimetic activity for multiple biomarkers monitoring, J. Anal. Test. 7 (2023) 53–68.
[82] S. Singh, N. Rai, H. Tiwari, et al., Recent advancements in the formulation of nanomaterials-based nanozymes, their catalytic activity, and biomedical applications, ACS Appl. Bio Mater. 6 (2023) 3577–3599.
[83] P. Liu, Y. Wang, L. Han, et al., Colorimetric assay of bacterial pathogens based on Co_3O_4 magnetic nanozymes conjugated with specific fusion phage proteins and magnetophoretic chromatography, ACS Appl. Mater. Interfaces 12 (2020) 9090–9097.
[84] M. He, J. Lin, O.U. Akakuru, et al., Octahedral silver oxide nanoparticles enabling remarkable SERS activity for detecting circulating tumor cells, Sci. China Life Sci. 65 (2022) 561–571.
[85] J. Lin, W. Ren, A. Li, et al., Crystal-amorphous core-shell structure synergistically enabling TiO_2 nanoparticles' remarkable SERS sensitivity for cancer cell imaging, ACS Appl. Mater. Interfaces 12 (2020) 4204–4211.
[86] J. Lin, J. Yu, O.U. Akakuru, et al., Low temperature-boosted high efficiency photo-induced charge transfer for remarkable SERS activity of ZnO nanosheets, Chem. Sci. 11 (2020) 9414–9420.
[87] O.S. Wolfbeis, An overview of nanoparticles commonly used in fluorescent bioimaging, Chem. Soc. Rev. 44 (2015) 4743–4768.
[88] Z. Li, G. Wang, Y. Shen, et al., DNA-templated magnetic nanoparticle-quantum dot polymers for ultrasensitive capture and detection of circulating tumor cells, Adv. Funct. Mater. 28 (2018), 1707152.
[89] P. Chen, Y. Wang, Y. He, et al., Homogeneous visual and fluorescence detection of circulating tumor cells in clinical samples via selective recognition reaction and enzyme-free amplification, ACS Nano 15 (2021) 11634–11643.
[90] P. Jia, C. Ding, Z. Sun, et al., DNA precisely regulated Au nanorods/Ag_2S quantum dots satellite structure for ultrasensitive detection of prostate cancer biomarker, Sensor. Actuator. B Chem. 347 (2021), 130585.
[91] A.B. Ganganboina, A. Dutta Chowdhury, R.A. Doong, N-doped graphene quantum dots-decorated V_2O_5 nanosheet for fluorescence turn off-on detection of cysteine, ACS Appl. Mater. Interfaces 10 (2018) 614–624.
[92] W. Zhou, Y. Han, B.J. Beliveau, et al., Combining qdot nanotechnology and DNA nanotechnology for sensitive single-cell imaging, Adv. Mater. 32 (2020), e1908410.
[93] K.T. Yong, W.C. Law, R. Hu, et al., Nanotoxicity assessment of quantum dots: from cellular to primate studies, Chem. Soc. Rev. 42 (2013) 1236–1250.
[94] R. Purbia, S. Paria, Yolk/shell nanoparticles: Classifications, synthesis, properties, and applications, Nanoscale 7 (2015) 19789–19873.
[95] R. Ding, Y. Chen, Q. Wang, et al., Recent advances in quantum dots-based biosensors for antibiotics detection, J. Pharm. Anal. 12 (2022) 355–364.
[96] G. Chen, H. Qiu, P.N. Prasad, et al., Upconversion nanoparticles: design, nanochemistry, and applications in theranostics, Chem. Rev. 114 (2014) 5161–5214.
[97] Z. Deng, S. Bi, M. Jiang, et al., Endogenous H_2S-activated orthogonal second near-infrared emissive nanoprobe for *in situ* ratiometric fluorescence imaging of metformin-induced liver injury, ACS Nano 15 (2021) 3201–3211.
[98] C. Hao, X. Wu, M. Sun, et al., Chiral core-shell upconversion nanoparticle@MOF nanoassemblies for quantification and bioimaging of reactive oxygen species *in vivo*, J. Am. Chem. Soc. 141 (2019) 19373–19378.
[99] J. Zhou, Q. Liu, W. Feng, et al., Upconversion luminescent materials: advances and applications, Chem. Rev. 115 (2015) 395–465.
[100] Y. Yang, L. Song, Y. Huang, et al., Asymmetrical molecular decoration of gold nanorods for engineering of shape-controlled AuNR@Ag core-shell nanostructures, Langmuir 35 (2019) 16900–16906.
[101] L. Jin, S. Shen, Y. Huang, et al., Corn-like Au/Ag nanorod-mediated NIR-II photothermal/photodynamic therapy potentiates immune checkpoint antibody efficacy by reprogramming the cold tumor microenvironment, Biomaterials 268 (2021), 120582.
[102] J. Reguera, J. Langer, D. Jiménez de Aberasturi, et al., Anisotropic metal nanoparticles for surface enhanced Raman scattering, Chem. Soc. Rev. 46 (2017) 3866–3885.
[103] W. Kim, S.H. Lee, J.H. Kim, et al., Paper-based surface-enhanced Raman spectroscopy for diagnosing prenatal diseases in women, ACS Nano 12 (2018) 7100–7108.
[104] C. Li, S. Li, A. Qu, et al., Directing arrowhead nanorod dimers for microRNA *in situ* Raman detection in living cells, Adv. Funct. Mater. 30 (2020), 2001451.
[105] S. Mokashi-Punekar, Y. Zhou, S.C. Brooks, et al., Construction of chiral, helical nanoparticle superstructures: progress and prospects, Adv. Mater. 32 (2020), e1905975.
[106] L. Song, Y. Huang, Z. Nie, et al., Macroscopic two-dimensional monolayer films of gold nanoparticles: fabrication strategies, surface engineering and functional applications, Nanoscale 12 (2020) 7433–7460.
[107] Y. Rong, L. Song, P. Si, et al., Macroscopic assembly of gold nanorods into superstructures with controllable orientations by anisotropic affinity interaction, Langmuir 33 (2017) 13867–13873.
[108] L. Chen, Y. Huang, L. Song, et al., Biofriendly and regenerable emotional monitor from interfacial ultrathin 2D PDA/AuNPs cross-linking films, ACS Appl. Mater. Interfaces 11 (2019) 36259–36269.
[109] H. Lin, L. Song, Y. Huang, et al., Macroscopic Au@PANI core/shell nanoparticle superlattice monolayer film with dual-responsive plasmonic switches, ACS Appl. Mater. Interfaces 12 (2020) 11296–11304.
[110] Q. Cheng, L. Song, H. Lin, et al., Free-standing 2D Janus gold nanoparticles monolayer film with tunable bifacial morphologies via the asymmetric growth at air-liquid interface, Langmuir 36 (2020) 250–256.
[111] J. Kim, M. Kim, M.S. Lee, et al., Wearable smart sensor systems integrated on soft contact lenses for wireless ocular diagnostics, Nat. Commun. 8 (2017), 14997.
[112] J.T. Reeder, J. Choi, Y. Xue, et al., Waterproof, electronics-enabled, epidermal microfluidic devices for sweat collection, biomarker analysis, and thermography in aquatic settings, Sci. Adv. 5 (2019), eaau6356.
[113] A. Garg, W. Nam, W. Zhou, Reusable surface-enhanced Raman spectroscopy membranes and textiles via template-assisted self-assembly and micro/nanoimprinting, ACS Appl. Mater. Interfaces 12 (2020) 56290–56299.
[114] H.J. Jeon, S. Kim, S. Park, et al., Optical assessment of tear glucose by smart biosensor based on nanoparticle embedded contact lens, Nano Lett. 21 (2021) 8933–8940.
[115] J.W. Jeong, M.M. Arnob, K.M. Baek, et al., 3D cross-point plasmonic nanoarchitectures containing dense and regular hot spots for surface-enhanced Raman spectroscopy analysis, Adv. Mater. 28 (2016) 8695–8704.
[116] D. Yang, S. Afroosheh, J.O. Lee, et al., Glucose sensing using surface-enhanced Raman-mode constraining, Anal. Chem. 90 (2018) 14269–14278.
[117] Y. Wang, C. Zhao, J. Wang, et al., Wearable plasmonic-metasurface sensor for noninvasive and universal molecular fingerprint detection on biointerfaces, Sci. Adv. 7 (2021), eabe4553.
[118] D.K. Kwon, J.M. Myoung, Wearable and semitransparent pressure-sensitive light-emitting sensor based on electrochemiluminescence, ACS Nano 14 (2020) 8716–8723.
[119] L. Wang, Q. Hou, W. Zheng, et al., Fluorescent and antibacterial aminobenzeneboronic acid (ABA)-modified gold nanoclusters for self-monitoring residual dosage and smart wound care, ACS Nano 15 (2021) 17885–17894.
[120] H. Huang, W. Feng, Y. Chen, Two-dimensional biomaterials: material science, biological effect and biomedical engineering applications, Chem. Soc. Rev. 50 (2021) 11381–11485.
[121] X. Cao, C. Ding, C. Zhang, et al., Transition metal dichalcogenide quantum dots: synthesis, photoluminescence and biological applications, J. Mater. Chem. B 6 (2018) 8011–8036.

[122] A. Bolotsky, D. Butler, C. Dong, et al., Two-dimensional materials in biosensing and healthcare: from *in vitro* diagnostics to optogenetics and beyond, ACS Nano 13 (2019) 9781–9810.
[123] J. Ping, Z. Fan, M. Sindoro, et al., Recent advances in sensing applications of two-dimensional transition metal dichalcogenide nanosheets and their composites, Adv. Funct. Mater. 27 (2017), 1605817.
[124] Y. Su, Q. Zhang, X. Miao, et al., Spatially engineered Janus hybrid nanozyme toward SERS liquid biopsy at nano/microscales, ACS Appl. Mater. Interfaces 11 (2019) 41979–41987.
[125] T. Xue, W. Liang, Y. Li, et al., Ultrasensitive detection of miRNA with an antimonene-based surface plasmon resonance sensor, Nat. Commun. 10 (2019), 28.
[126] H. Lin, Y. Wang, S. Gao, et al., Theranostic 2D tantalum carbide (MXene), Adv. Mater. 32 (2020), e2003085.
[127] D. Ji, Y. Zhang, Y. Zang, et al., Targeted intracellular production of reactive oxygen species by a 2D molybdenum disulfide glycosheet, Adv. Mater. 28 (2016) 9356–9363.
[128] P. Li, F. Cheng, W. Xiong, et al., New synthetic strategies to prepare metal–organic frameworks, Inorg. Chem. Front. 5 (2018) 2693–2708.
[129] X. Qiao, B. Su, C. Liu, et al., Selective surface enhanced Raman scattering for quantitative detection of lung cancer biomarkers in superparticle@MOF structure, Adv. Mater. 30 (2018), 1702275.
[130] P. Falcaro, R. Ricco, A. Yazdi, et al., Application of metal and metal oxide nanoparticles@MOFs, Coord. Chem. Rev. 307 (2016) 237–254.
[131] T. Gong, Q. Sui, P. Li, et al., Versatile and switchable responsive properties of a lanthanide-viologen metal-organic framework, Small 15 (2019), e1803468.
[132] Y. Yu, X. Zhang, J. Ma, et al., Cu(I)-MOF: Naked-eye colorimetric sensor for humidity and formaldehyde in single-crystal-to-single-crystal fashion, Chem. Commun. 50 (2014) 1444–1446.
[133] Y. Liu, X. Xie, C. Cheng, et al., Strategies to fabricate metal–organic framework (MOF)-based luminescent sensing platforms, J. Mater. Chem. C 7 (2019) 10743–10763.
[134] Y. Li, J. Li, D. Zhu, et al., 2D Zn-porphyrin-based Co(II)-MOF with 2-methylimidazole sitting axially on the paddle-wheel units: an efficient electrochemiluminescence bioassay for SARS-CoV-2, Adv. Funct. Mater. 32 (2022), 2209743.
[135] M. Guo, Z. Jin, J. Pan, et al., Construction of COFs@MoS_2-Pd hierarchical tubular heterostructures for enhanced catalytic performance, Inorg. Chem. 63 (2024) 18263–18275.
[136] Y. Li, F. Yang, R. Yuan, et al., Electrochemiluminescence covalent organic framework coupling with CRISPR/Cas12a-mediated biosensor for pesticide residue detection, Food Chem. 389 (2022), 133049.
[137] N. Panwar, A.M. Soehartono, K.K. Chan, et al., Nanocarbons for biology and medicine: sensing, imaging, and drug delivery, Chem. Rev. 119 (2019) 9559–9656.
[138] E. Shuang, C. He, J. Wang, et al., Tunable organelle imaging by rational design of carbon dots and utilization of uptake pathways, ACS Nano 15 (2021) 14465–14474.
[139] Y. Peng, C. Ye, R. Yan, et al., Activatable core-shell metallofullerene: an efficient nanoplatform for bimodal sensing of glutathione, ACS Appl. Mater. Interfaces 11 (2019) 46637–46644.
[140] M. Xu, S. Xing, Y. Zhao, et al., Peptide nucleic acid-assisted colorimetric detection of single-nucleotide polymorphisms based on the intrinsic peroxidase-like activity of hemin-carbon nanotube nanocomposites, Talanta 232 (2021), 122420.
[141] Y. Guo, L. Deng, J. Li, et al., Hemin-graphene hybrid nanosheets with intrinsic peroxidase-like activity for label-free colorimetric detection of single-nucleotide polymorphism, ACS Nano 5 (2011) 1282–1290.
[142] M. Li, T. Chen, J.J. Gooding, et al., Review of carbon and graphene quantum dots for sensing, ACS Sens. 4 (2019) 1732–1748.
[143] D.A. Hopper, R.R. Grote, S.M. Parks, et al., Amplified sensitivity of nitrogen-vacancy spins in nanodiamonds using all-optical charge readout, ACS Nano 12 (2018) 4678–4686.
[144] A. Antonucci, J. Kupis-Rozmysłowicz, A.A. Boghossian, Noncovalent protein and peptide functionalization of single-walled carbon nanotubes for biodelivery and optical sensing applications, ACS Appl. Mater. Interfaces 9 (2017) 11321–11331.
[145] C.A.S. Ballesteros, L.A. Mercante, A.D. Alvarenga, et al., Recent trends in nanozymes design: from materials and structures to environmental applications, Mater. Chem. Front. 5 (2021) 7419–7451.
[146] L. Deng, M. Zhu, Metal–nitrogen (Co-g-C_3N_4) doping of surface-modified single-walled carbon nanohorns for use as an oxygen reduction electrocatalyst, RSC Adv. 6 (2016) 25670–25677.
[147] J. Kim, S.J. Park, D.H. Min, Emerging approaches for graphene oxide biosensor, Anal. Chem. 89 (2017) 232–248.
[148] J. Bartelmess, S.J. Quinn, S. Giordani, Carbon nanomaterials: multi-functional agents for biomedical fluorescence and Raman imaging, Chem. Soc. Rev. 44 (2015) 4672–4698.